Nonadiabatic effects in C–Br bond scission in the photodissociation of bromoacetyl chloride

Rosendo Valero and Donald G. Truhlar[a)]
Department of Chemistry, University of Minnesota, Minneapolis, Minnesota 55455 and Supercomputing Institute, University of Minnesota, Minneapolis, Minnesota 55455

(Received 7 August 2006; accepted 22 September 2006; published online 16 November 2006)

Bromoacetyl chloride photodissociation has been interpreted as a paradigmatic example of a process in which nonadiabatic effects play a major role. In molecular beam experiments by Butler and co-workers [J. Chem. Phys. **95**, 3848 (1991); J. Chem. Phys. **97**, 355 (1992)], $BrCH_2C(O)Cl$ was prepared in its ground electronic state (S_0) and excited with a laser at 248 nm to its first excited singlet state (S_1). The two main ensuing photoreactions are the ruptures of the C–Cl bond and of the C–Br bond. A nonadiabatic model was proposed in which the C–Br scission is strongly suppressed due to nonadiabatic recrossing at the barrier formed by the avoided crossing between the S_1 and S_2 states. Recent reduced-dimensional dynamical studies lend support to this model. However, another interpretation that has been given for the experimental results is that the reduced probability of C–Br scission is a consequence of incomplete intramolecular energy redistribution. To provide further insight into this problem, we have studied the energetically lowest six singlet electronic states of bromoacetyl chloride by using an *ab initio* multiconfigurational perturbative electronic structure method. Stationary points (minima and saddle points) and minimum energy paths have been characterized on the S_0 and S_1 potential energy surfaces. The fourfold way diabatization method has been applied to transform five adiabatic excited electronic states to a diabatic representation. The diabatic potential energy matrix of the first five excited singlet states has been constructed along several cuts of the potential energy hypersurfaces. The thermochemistry of the photodissociation reactions and a comparison with experimental translational energy distributions strongly suggest that nonadiabatic effects dominate the C–Br scission, but that the reaction proceeds along the energetically allowed diabatic pathway to excited-state products instead of being nonadiabatically suppressed. This conclusion is also supported by the low values of the diabatic couplings on the C–Br scission reaction path. The methodology established in the present study will be used for the construction of global potential energy surfaces suitable for multidimensional dynamics simulations to test these preliminary interpretations. © *2006 American Institute of Physics*.
[DOI: 10.1063/1.2363991]

I. INTRODUCTION

The theoretical treatment of most thermally initiated chemical reactions invokes the Born-Oppenheimer (BO) approximation, in which the electronic and nuclear motions are separated and the nuclei evolve on a single adiabatic potential energy surface (PES), usually the ground adiabatic PES. Photoexcitation of a chemical system in the visible and ultraviolet regions of the spectrum usually accesses electronically excited states. The subsequent dynamics often involves nonradiative electronic transitions to other excited states or to the ground state. Transitions between electronic states imply a breakdown of the Born-Oppenheimer approximation, leading to so-called non-Born-Oppenheimer (non-BO) or electronically nonadiabatic processes. Theoretical methods designed to treat such processes have more complications than those used to study BO reactions, but they have experienced considerable progress in recent years.[1] Electronically nonadiabatic effects are at the heart of many chemical processes, including electron transfer, collisional deactivation of electronically excited species, chemiluminescence, and many processes initiated by electronic impacts (e.g., dissociative electron attachment and recombination in electron-molecule scattering or processes analogous to photochemistry but initiated by electron impact rather than photon impact), as well as many biochemical processes such as vision, light transduction in photosynthesis, and photostability of nucleic acid bases. It is now well established that conical intersections of potential energy surfaces are often the features that mediate electronically nonadiabatic events such as fast nonradiative decay of electronically excited species.[2–6]

The theoretical treatment of nonadiabatic effects depends on the choice of representation for the electronic Hamiltonian of the system. The wave function for a molecular system (electrons and nuclei) can be expressed in terms of products of electronic and nuclear basis functions. The electronic basis functions may be taken as eigenfunctions of the electronic Hamiltonian (the so-called adiabatic basis). In this representation, the adiabatic states are coupled by nuclear momentum and kinetic energy, and the coupling matrix elements are called nonadiabatic coupling terms (NACTs).

a)Electronic mail: truhlar@umn.edu

Adiabatic wave functions and NACTs are known to be rapidly varying functions of the nuclear coordinates in regions of close proximity of PESs, with singularities at conical intersections, and NACTs, as well as being matrix elements in electronic state space, are $(3N-6)$-dimensional vectors in real space, where N is the number of atoms. For these reasons, it is usually more convenient to transform the adiabatic wave functions to the diabatic representation. Although strictly diabatic states do not exist in general,[7] it is possible, when the geometry is far from conical intersections, to construct diabatic states for which the NACTs are as small, in order of magnitude, as the non-BO terms are when the BO approximation is a good approximation.[8] Diabatic states are smooth functions of the nuclear coordinates that keep their essential character over the entire nuclear configuration space, and they are constructed so as to reduce the magnitude of the NACTs to a negligible level. These states should strictly be called quasidiabatic states, but following the accepted convention we will refer to quasidiabatic states as diabatic states. Unlike the adiabatic electronic Hamiltonian, the diabatic electronic Hamiltonian is not diagonal; it contains the diabatic potential energy surfaces on the diagonals and their scalar potential couplings as off-diagonal elements. Several methods, some being of greater generality than others, have been proposed to carry out the transformation from the adiabatic basis to a diabatic basis.[9–30]

Photodissociation reactions that have more than one energetically allowed product raise interesting questions regarding the factors that control the branching ratio between the photoproducts and regarding the possibility of achieving selective dissociation to a particular product. In order to elucidate these issues, Butler and co-workers have undertaken extensive experimental and theoretical studies of many photodissociation reactions.[31–41] To rationalize the experimental observations, they developed a model that identifies reactions that proceed close to a conical intersection and Woodward-Hoffmann (WH)-forbidden[42] reactions as classes of reactions particularly prone to nonadiabatic effects. Whereas the role of conical intersections in promoting nonadiabatic effects has long been recognized (see above), this is not the case for WH-forbidden reactions. The model proposes that in WH-forbidden reactions, the configuration interaction matrix elements that control the magnitude of the diabatic couplings at the avoided crossing forming the adiabatic reaction barrier are anomalously small. This leads to a type of nonadiabatic effect known as nonadiabatic recrossing or diabatic trapping and a reduced yield of photoproducts when compared to models that assume the reactions to proceed adiabatically, such as the statistical Rice-Ramsperger-Kassel-Marcus (RRKM) theory. One way of computing an approximate probability of nonadiabatic transitions is using the well-known one-dimensional Landau-Zener model.[43] This model has been successfully applied to several systems.[44] However, it should be used with caution, especially to treat multidimensional reactions, for which it has been shown in some cases to deviate strongly from the exact quantum results.[45]

Scission of the C–Br bond in bromoacetyl chloride $[BrC_\alpha H_2C(O)Cl]$ has been interpreted as a WH-forbidden reaction with suppression of reactivity due to nonadiabatic recrossing. Note that throughout the article, the carbonyl carbon is called C and the other carbon is called C_α (except for naming structures in figures where the "α" would be too small). In crossed laser-molecular beam studies of photodissociation from ground-state $BrC_\alpha H_2C(O)Cl$,[31,32,34,36] a laser at 248 nm (5.00 eV) excites the overlapping $^1[n(O)\rightarrow\pi^*(C{=}O)]$ and $^1[n(Br)\rightarrow\sigma^*(C_\alpha{-}Br)]$ electronic transitions. The main photoreactions are the scission of the C_α–Br and C–Cl bonds. In order to isolate the outcome of excitation to the S_1 state, the direct C_α–Br rupture due to partial excitation of the $^1[n(Br)\rightarrow\sigma^*(C_\alpha{-}Br)]$ band was subtracted from the total experimental signal. The dynamics following $^1[n(O)\rightarrow\pi^*(C{=}O)]$ excitation shows a clear preference for breaking the stronger α C–Cl bond over the weaker β C_α–Br bond. The branching ratio of C–Cl to C_α–Br dissociation was found to be 1.0:0.4, in contrast to the prediction of the RRKM theory that the C_α–Br rupture should be strongly favored.

To gain insight into the origin of the preference for rupture of the C–Cl bond in $BrC_\alpha H_2C(O)Cl$, Butler and co-worker[33,36] performed *ab initio* configuration interaction singles and doubles (CISD) calculations of the electronic ground-state energies. Excitation energies were computed at the configuration interaction singles (CIS) level and added to the CISD ground-state energies to construct the PESs of the first and second electronically excited singlet states. The molecule was assumed to retain the *trans*-C_s conformation of the ground-state minimum. The model treats each of the carbon-halogen adiabatic bond dissociations as arising from a separate two-state intersection involving the S_1 and S_2 electronic states. Several carbon-halogen dissociation curves were constructed, each for a particular value of the C–O bond distance. The calculations showed that the magnitude of the diabatic coupling is smaller for the intersection involving the C_α–Br bond than for the intersection involving the C–Cl bond at relatively short and long C–O bond distances. The preference for C–Cl rupture was proposed to arise from nonadiabatic recrossing effects being larger in the C_α–Br channel, favoring C–Cl dissociation despite its much higher adiabatic barrier.

Recent theoretical studies[46–48] support the model of Butler and co-workers for $BrC_\alpha H_2C(O)Cl$. Quantum wave packet calculations in one dimension[46] (1D) and two dimensions[47] (2D) were carried out by Bacchus-Montabonel *et al.*[46] and Lasorne *et al.*[47] using the complete active space self-consistent field[49–51] (CASSCF) method to calculate reduced-dimensional PESs. The 1D studies included only the C–Cl or C_α–Br coordinates, while the 2D studies included either the $[C_\alpha{-}Br, C{=}O]$ or the [C–Cl, C=O] subsets of coordinates. The authors found a Cl:Br branching ratio in agreement with experiment in their 2D calculations. However, the value of the mean energy distributed to each of the above 2D coordinate subsets was found to have a strong influence on the computed ratio. Nonadiabatic transition-state theory calculations by Marks[48] based on the electronic structure calculations of Kash *et al.*[35] also yielded branching ratios in reasonable agreement with experiment.

An opposite conclusion was reached in a recent CASSCF and multireference configuration interaction (MRCI) study by Ding *et al.*[52] These authors concluded that nonadiabaticity should not play an important role in the reaction. The large nonadiabatic effects predicted in previous research would be a consequence of the underestimation of the diabatic couplings and overestimation of the barrier heights. Based on these observations, Ding *et al.* suggested that the main factor responsible for the preference of C–Cl over C_α–Br photodissociation is incomplete intramolecular energy redistribution. The latter effect would cause the preferential rupture of the C–Cl bond because it is nearer than the C_α–Br bond to the initially excited C=O chromophore.

In this contribution we present an *ab initio* electronic structure study of the six lowest singlet PESs of bromoacetyl chloride with the goal of further elucidating the mechanistic features of its photodissociation. Section II presents the electronic structure methods, which involve many-electron basis functions, called configuration state functions (CSFs), constructed from appropriately chosen one-electron molecular orbitals (MOs), which in turn are expressed in terms of a one-electron Gaussian basis set. The space spanned by the orbitals is optimized for a reference wave function in a first step, and dynamical correlation of the electrons is introduced in a second step. The presentation in Sec. II emphasizes (i) the selection of the active space that determines the space spanned by the CSFs in the reference function and (ii) the subsequent fourfold way[26,53,54] diabatization procedure. Section III characterizes the stationary points and reaction paths on the S_0 and S_1 PESs. The fourfold way is applied to transform the five first excited adiabatic states to the diabatic representation. Diabatic energies and couplings are presented along several cuts of the full-dimensional PESs. In Sec. IV the present results are compared with previous theoretical studies, and the role of nonadiabatic effects in the system is discussed. Section V presents conclusions.

II. METHODOLOGY

II.A. Electronic structure methods

The first task one confronts in the theoretical study of photodissociation reactions is to choose electronic structure methods suitable for the description of the wave functions and potential energy surfaces of excited electronic states. It is often necessary to include more than one CSF even for a correct zeroth-order description of such states. Methods in which the orbitals are optimized simultaneously with the configurational coefficients are called multiconfigurational self-consistent field (MCSCF) methods.[55] The most systematic choice of configurations to include in a MCSCF calculation is a full CI in a small set of orbitals called the active space; this yields the CASSCF method.[49–51] One drawback of the CASSCF method is that it does not include dynamical correlation. This leads to inaccuracies in reaction energies, barrier heights, and vertical excitation energies. The missing dynamical correlation is best introduced using MRCI methods[56–60] or multireference perturbation theory (MRPT) methods[61–69] (multireference methods use a MCSCF wave function as a zero-order function, called the reference state). Although MRCI is in principle capable of yielding results close to the full-CI limit,[59] in the space of all orbitals (not just the active space), the rapid increase of the computational expense with the size of the system prevented its use for the present exploratory study, and so we employed MRPT. For larger systems, MRPT is usually the method of choice. To deal with regions of near degeneracy of adiabatic electronic states, MRPT methods of the effective Hamiltonian type are most suitable.[63,65,68] In this study we have employed such a method, namely, multiconfigurational quasidegenerate perturbation theory (MC-QDPT) at second order[63,69] with a CASSCF wave function as the reference state. Not only are CASSCF and MC-QDPT multiconfigurational methods, they are also multistate methods; that is, they simultaneously yield energies and wave functions for more than one electronic state. If the orbitals and configurational coefficients were optimized to minimize the energy of a single state, the treatment would be unbalanced. Therefore, for calculations designed to explore coupled potential energy surfaces, one optimizes to minimize the average error of electronic states of interest.[70–73]

II.B. Adiabatic states and orbitals of bromoacetyl chloride

The observed anisotropy parameters for the Cl atom ($\beta = 1.0 \pm 0.3$) and the Br atom ($\beta = 0.6 \pm 0.3$) were interpreted in the experiments as signaling that the dissociation proceeds on a fast time scale with an upper limit of 1 ps.[32] This implies that intersystem crossing to triplet states and internal conversion to the ground electronic state are not competitive with direct dissociation on the S_1 PES (excluding $S_1 \rightarrow S_0$ transitions in C_α–Br and C–Cl asymptotic regions where an atom is almost free and S_1 and S_0 are nearly degenerate). Therefore, in the present article, we have only studied the singlet states, leaving aside the question of whether triplet states might play any role in the photodissociation. In addition, only states of valence character have been considered, that is, states that have Rydberg character were not taken into account. This choice is based on a comparison to systems such as CH_2BrCl (Ref. 74) and CF_2BrCl,[75] for which the lowest Rydberg states are more than 7 eV above the ground-state energy in the Franck-Condon region. Finally, scalar relativistic effects and spin-orbit (SO) coupling are not included in our theoretical treatment. Although the Br spin-orbit splitting [0.46 eV (Ref. 76)] affects the dissociation energies significantly, its effect on the Cl:Br branching ratio may be omitted in a qualitative discussion since photodissociation to products takes place with a large amount of available energy (see below) and because the experiments with which we are concerned do not determine branching ratios to the different fine-structure electronic states of Cl or Br.[31,32,34,36]

The crucial step in the application of CASSCF and methods based on CASSCF is the selection of the active space. We aimed to define the minimal active space that can correctly describe the excited electronic states associated with the three chromophores (C=O group, Br atom, and Cl atom) in the $BrC_\alpha H_2C(O)Cl$ molecule and the competitive

C_α–Br and C–Cl bond ruptures. The S_1 state has $^1[n(O)\pi^*(C{=}O)]$ as its dominant configuration close to the ground-state equilibrium geometry, and the states that can intersect with the S_1 PES have $^1[n(X)\sigma^*(C{-}X)]$ and $^1[n'(X)\sigma^*(C{-}X)]$ (X=Br,Cl) as their dominant configurations. In this notation, $n(O)$, $n(X)$, and $n'(X)$ are orbitals of nonbonding character centered on the respective atoms. Thus, the active space must at least contain the $n(O)$, $n(Br)$, $n'(Br)$, $n(Cl)$, $n'(Cl)$, $\pi^*(C{=}O)$, $\sigma^*(C_\alpha{-}Br)$, and $\sigma^*(C{-}Cl)$ molecular orbitals. Furthermore, the correct description of the C_α–Br and C–Cl bond dissociations requires including the bonding $\sigma(C_\alpha{-}Br)$ and $\sigma(C{-}Cl)$ MOs; also, due to the partial rupture of the carbonyl π bond in the S_1 state, the $\pi(C{=}O)$ MO must be included along with the $\pi^*(C{=}O)$ MO in the active space. Thus, the active space chosen is composed of the following 11 MOs: $\{\pi(C{=}O)$, $n(O)$, $\sigma(C_\alpha{-}Br)$, $n(Br)$, $n'(Br)$, $\sigma(C{-}Cl)$, $n(Cl)$, $n'(Cl)$, $\pi^*(C{=}O)$, $\sigma^*(C_\alpha{-}Br)$, $\sigma^*(C{-}Cl)\}$. The ground-state configuration at the ground-state equilibrium geometry is a closed-shell singlet and can be described as

$$[(\text{inactive})^{58}\ \pi(C{=}O)^2\ n(O)^2\ \sigma(C_\alpha{-}Br)^2\ n(Br)^2\ n'(Br)^2\ \sigma(C{-}Cl)^2 n(Cl)^2 n'(Cl)^2\ \pi^*(C{=}O)^0\ \sigma^*(C_\alpha{-}Br)^0\ \sigma^*(C{-}Cl)^0].$$

Here "inactive" simply stands for the 29 lowest-energy MOs, which are doubly occupied and are not included in the active space. In the CASSCF calculation, 16 active electrons are distributed in all possible ways among the 11 active MOs, so we will refer to this active space as the (16,11) active space. Note that this active space cannot describe the rupture of the $C{-}C_\alpha$ bond. The experiments showed that the carbon-carbon bond dissociation has a rate equal to only about 10% of the rate of C–Cl dissociation.[37] We believe it is not unreasonable to exclude the carbon-carbon bond dissociation process from consideration because it is not expected to affect the competition between the C_α–Br and C–Cl dissociations.

Geometry optimizations to locate minima and saddle points on the S_0 and S_1 PESs were performed at the state-specific (SS) CASSCF level, whereas for calculations on the coupled surfaces, the energies of the six lowest-energy singlet electronic states were averaged with equal weights in the CASSCF calculations. Henceforth we will refer to state-specific CASSCF(16,11)/6-31G(d,p) calculations as SS-CASSCF, and state-average CASSCF(16,11)/6-31G(d,p) calculations will be denoted SA-CASSCF.

A first-order convergence algorithm[77] was used to compute the CASSCF wave functions in order to keep the orbital composition of the active space fixed for all nuclear configurations. First-order algorithms are based on the orbital gradient, whereas second-order algorithms use both the orbital gradient and Hessian.[51] Although not as efficient as second-order algorithms, the first-order algorithm used prevents the interchange of the initial active orbitals with inactive and virtual orbitals. In the present case, some natural orbital occupation numbers are close to 2.0 or 0.0 in some regions of configuration space, and the first-order algorithm was essential in defining the active orbitals consistently throughout the PESs.

The 6-31G(d,p) Gaussian basis set[78] was used in the CASSCF and MC-QDPT calculations with five spherical harmonic d functions for nonhydrogenic atoms.

Dynamical correlation was introduced using the MC-QDPT method with a SA-CASSCF reference wave function. All MC-QDPT calculations are based on a six-state effective Hamiltonian, denoted 6S, or a two-state effective Hamiltonian, denoted 2S. Note that in this paper, 6S-MC-QCPT calculations are always based on SA(6)-CASSCF orbitals, and 2S-MC-QDPT calculations are always based on SA(2)-CASSCF orbitals, where the value in parentheses is the number of states averaged in the CASSCF step. The CASSCF and MC-QDPT calculations were performed without any symmetry constraints on the wave functions.

To avoid artifacts due to intruder states in the MC-QDPT wave function, the intruder state avoidance (ISA) method[79] was used in the calculation of the energies of the stationary points as well as of some reduced-dimensionality cuts along the potential energy hypersurfaces. The level shift parameter[79] b of the ISA method was set to $0.02E_h^2$ (note: $1E_h \equiv 1$ hartree).

To estimate the adequacy of calculating excitation energies obtained at the MC-QDPT level, the multistate equation-of-motion[80] coupled cluster method with single and double excitations[81–84] (EOM-CCSD) was employed with the same 6-31G(d,p) basis set. Dissociation energies from the absolute minimum on the ground-state potential to products were computed by a single-state method,[85] namely, partially spin-restricted open-shell coupled-cluster theory[86,87] with single and double excitations and quasiperturbative estimation[88] of the triples contribution [RCCSD(T)] level, and were also compared with the dissociation energies obtained at the MC-QDPT level. The RCCSD(T) calculations were performed with correlation consistent polarized valence double zeta (cc-pVDZ) and correlation consistent polarized triple zeta (cc-pVTZ) basis sets,[89] and the results were extrapolated to the infinite basis (IB) limit using an approach explained elsewhere.[90,91] This method with the extrapolation parameters taken from Ref. 91 will be denoted RCCSD(T)/IB. The 1s atomic orbitals of the two carbon atoms and of the oxygen atom, the 1s, 2s, and 2p atomic orbitals of the chlorine atom, and the 1s, 2s, 2p, 3s, 3p, and 3d atomic orbitals of the bromine atom (a total of 22 orbitals) were uncorrelated (frozen) in the MC-QDPT, EOM-CCSD, and RCCSD(T) calculations.

The CASSCF and MC-QDPT calculations were carried

out using HONDOPLUS V4.7.[92,93] The EOM-CCSD calculations employed the ACESII program,[94] and the MOLPRO electronic structure package[95] was used for the RCCSD(T) calculations.

II.C. Fourfold way diabatization method

The diabatization method[26,53,54] that we use is based on the configurational uniformity concept of Atchity and Ruedenberg.[22,96,97] The key principles of the method are the construction of suitable diabatic MOs (DMOs) and their use to construct diabatic configuration state functions (DCSFs) that are employed to enforce configurational uniformity on the multiconfiguration wave function of the CASSCF or MC-QDPT step. The DMOs and the DCSFs must have two properties:[26] (1) they must be uniquely defined at each nuclear configuration and be smooth along continuous nuclear-coordinate paths and (2) when the multiconfigurational wave functions are expressed in terms of DMOs, each state must be dominated by no more than a few DCSFs in regions where the electronic states are weakly interacting. The fourfold way method for constructing DMOs is based on the use of one-electron density matrices and transition density matrices to define the following functional:

$$D_3(\alpha_N,\alpha_R,\alpha_T)=\alpha_N D^{\mathrm{NO}}+\alpha_R D^{\mathrm{ON}}+\alpha_T D^{\mathrm{TD}}. \quad (1)$$

In Eq. (1) α_N,α_R, and α_T are parameters usually set to the values 2, 1, and 0.5 (we use the standard values in the present work), D^{NO} is a natural orbital density matrix, D^{ON} an occupation number density matrix, and D^{TD} a transition density matrix. The criterion for constructing DMOs based on maximization of the D_3 functional is called the threefold density criterion. In some cases, including the system treated in the present article, the configurational uniformity needs to be supplemented by additional constraints on MO uniformity to ensure the satisfaction of condition (1) above. This is done by introducing a set of λ reference MOs and defining a new term, called the reference overlap term, which contains an overlaplike quantity between the MOs at the current geometry and the reference MOs. When one or more reference MO is included it is called fourfold way, since it depends on the three functionals in Eq. (1) and on the set of reference MOs.

The DMOs are used to construct orthonormal DCSFs which are distributed into groups, with each group spanning a characteristic subspace that defines a diabatic state.[26,53,54] The basic requirement is that the group list (the group list is the list of DCSFs that defines a particular group) be the same for all nuclear geometries. The adiabatic many-electron wave functions are finally expressed in the basis of the DCSFs, and their CI coefficients are used to define the adiabatic-to-diabatic transformation matrix **T**. The equation that relates the adiabatic and diabatic energies is then

$$\mathbf{U}=\mathbf{T}^{\dagger}\mathbf{H}\mathbf{T}, \quad (2)$$

where **U** is the diabatic energy matrix with elements $\{U_{ij},i,j\leqslant N\}$, where the diagonal elements are the diabatic PESs and the off-diagonal elements are the diabatic couplings, and **H** is a diagonal matrix containing the adiabatic energies $\{E_i,i\leqslant N\}$. Diagonalization of the diabatic energy matrix **U** gives back the adiabatic energy matrix **H**.

Note that **T** and hence the diabatic energy matrix are defined up to a change in sign of one or more rows and columns; the signs are chosen arbitrarily at a certain nuclear configuration of one of the pathways, where the diabatic couplings have a non-negligible magnitude. Then the signs are chosen at all other geometries to make the diabatic couplings be continuous functions of geometry. In order to accomplish this and also to make a required one-to-one correspondence of the DMOs at one geometry with those at another, we proceed as follows. First, one or more reference geometries are chosen in the weak interaction regions, where diabatic states are equal to adiabatic states to a good approximation. The threefold way is carried out at each of the reference geometries and if necessary, some of the DMOs are defined as reference DMOs for the subsequent steps. The procedure is advanced by taking several consecutive geometries separated by sufficiently small steps along a certain pathway in nuclear configuration space, for instance, one that connects reactants and products. These paths are used only for ordering the DMOs obtained at a certain nuclear configuration so they have a one-to-one correspondence with the DMOs at the previous configuration and for determining the signs of off-diagonal elements of **U** to avoid discontinuities in the diabatic couplings as a function of the nuclear coordinates. A global exploration of the PESs and couplings can then be carried out by repeating this procedure along other pathways, for instance, connecting the different stationary points. For example, a third pathway is constructed that connects a nuclear configuration on the first pathway to one on the second pathway. The process is repeated until all orbital orderings and signs are consistent across all pathways on the PESs.

The fourfold way has the advantage that the diabatic states can be dominated by different DCSFs in different arrangements; this feature is crucial for constructing global PESs for multiarrangement systems. The fourfold way is applicable both at the CASSCF level and with electronic structure methods such as MC-QDPT that incorporate dynamical correlation.[53] Very recently the method has been applied in our group to the construction of global diabatic PESs for the ground and first excited electronic states of NH_3.[98,99]

II.D. Application of the fourfold way to bromoacetyl chloride

The first step in the application of the fourfold way to the $BrC_{\alpha}H_2C(O)Cl$ system is to establish a standard orientation so that the Cartesian coordinates of the atoms are uniquely and continuously defined at all nuclear configurations. In the standard orientation, the molecule is situated with the two carbon atoms and the Cl atom in the xz plane. Furthermore, the Cl atom is put at the origin with the C–Cl bond pointing to the negative direction of the z axis, and the C_{α} atom has a negative value of x. The threefold way was first applied along the C–Cl and C_{α}–Br stretching coordinates connecting some of the minima on the S_1 PES with the product fragments. However, it was found that configurational uniformity was not well fulfilled along these pathways

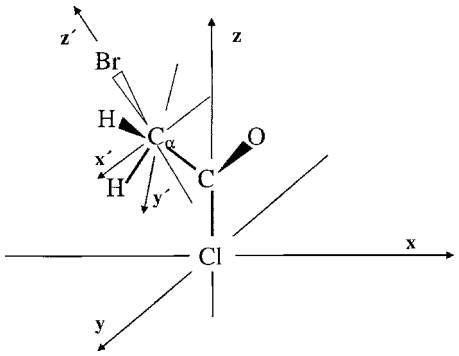

SCHEME 1. Standard (**xyz** coordinate system) and specific (**x′y′z′** coordinate system) orientations for the $BrC_{\alpha}H_2C(O)Cl$ molecule (see text).

due to the mixing of the DMOs that represent the nonbonding p orbitals of the halogen atoms when the bonds are stretched. As a consequence, the diabatic couplings showed an irregular dependence on the C–Cl and C_{α}–Br coordinates. To solve this problem, the more general fourfold way diabatization scheme was employed. Since the three orbitals of each halogen atom can mix among themselves when the carbon-halogen bonds are stretched, two orbitals per halogen for a total of four reference DMOs (Ref. 26) are necessary and sufficient to differentiate the DMOs. For a general molecular geometry, the Br atom is oriented arbitrarily with respect to the z axis and the xz plane of the standard orientation. In this situation, in order to keep the character of the reference DMOs fixed it becomes necessary to define them in a specific molecular orientation (denoted by primed coordinates), and for a general molecular geometry they must be transformed to the standard orientation (unprimed).[54] The specific orientation for the Br atom is defined as follows: the z' axis is defined as being parallel to the C_{α}–Br bond, the $x'z'$ plane is set to coincide with the Br,C_{α},C plane, and the y' axis is orthogonal to the $x'z'$ plane. The standard and specific orientations are shown in Scheme 1. Since the Cl atom is always situated at the coordinate origin, no reorientation of its reference DMOs is required. Therefore, the specific orientation for the Cl atom coincides with the standard orientation.

The four reference DMOs have been defined as those DMOs representing the nonbonding p orbitals in the specific orientations, that is, the Cl($p_{x'}$), Cl($p_{y'}$), Br($p_{x'}$), and Br($p_{y'}$) orbitals. In order to have reference DMOs that are geometry independent, the reference DMOs are computed at a geometry where the C–Cl and C_{α}–Br bond lengths are stretched one at a time to 5.0 Å with the rest of the geometrical parameters fixed at arbitrary values (since they do not influence the halogen atoms' DMOs), and the threefold way is carried out. The coefficients of the p_x- and p_y-type atomic orbitals of the Cl and Br atoms define the reference DMOs with the rest of the coefficients set to zero.

An additional complication that can be encountered even after reference DMOs are defined is that the character and order of the virtual DMOs change along the dissociation pathways. The origin of this problem is the coordinate-dependent mixing of the virtual DMOs, which prevents them from being consistently ordered along a whole dissociation pathway. The characters of the virtual DMOs when the $BrC_{\alpha}H_2C(O)Cl$ molecule contains a plane of symmetry and the bonds are not stretched are π^*(C═O), σ^*(C_{α}–Br), and σ^*(C–Cl). When the molecule contains a plane of symmetry only the two DMOs that have the same symmetry, namely, the σ^*(C_{α}–Br) and σ^*(C–Cl) DMOs, can mix with each other. The situation is more involved for nonsymmetric configurations because then the three DMOs can and do mix with each other. One way to tackle this problem would be to proceed along the same lines as done above for the DMOs of the halogens, i.e., at least two suitable additional reference DMOs for the virtual orbitals could be defined. Since the mixing between the virtual DMOs behaves continuously along the dissociation curves, a simpler solution was found, i.e., to include in the diabatic groups all the different orderings of the DMOs that represent the same CSF. In order to do this, it was found to be convenient to exclude the ground state from the diabatization procedure. The ground state can be kept as an adiabatic state, uncoupled to the other states for the present problem, because as explained above, the fast time scale of dissociation implies that internal conversion to the ground state should not be relevant to determining the Cl:Br branching ratio.[36] When the ground state is excluded and the diabatic group lists accommodate the multiple orderings of the virtual DMOs, their mixing along the C_{α}–Br and C–Cl coordinates is no longer a problem.

The fourfold way diabatization procedure was applied to the SA-CASSCF and MC-QDPT adiabatic wave functions and energies. To carry out an exploration of all the regions that are expected to be relevant to the dynamics up to potential energies of 5 eV, three types of pathways were constructed. The first type includes unrelaxed dissociation pathways starting at the geometries of the different minima on the S_0 and S_1 PESs, in which only the C–Cl or the C_{α}–Br bond distances are varied. In order to compare with previous work, one of the unrelaxed dissociation pathways is started at the geometry of an S_1 transition state (*trans-C_s* TS10, see below). The second type of pathway consists of hybrid linear-synchronous-transit/bond stretch pathways. The linear-synchronous-transit[100] section of the paths is constructed such that it connects the bond scission transition states to the minima on the S_1 PES and extends into the product channel up to a C–Br or C–Cl distance of about 3 Å. The bond stretch part of the paths consists of constant bond distance increments between 3 and 4 Å with the rest of the coordinates fixed. The third type consists of linear-synchronous-transit pathways that connect geometries close to the state intersection between the S_1, S_2, and S_3 states for the two different pathways of types 1 or 2. The purpose of the latter type of path is to achieve a unique definition of the sign of the diabatic couplings throughout the PESs, as explained above.

The fourfold way was performed using HONDOPLUS v4.7,[92,93] with minor changes to the code in order to exclude the ground state from diabatization and with the addition of the ISA algorithm from the version in GAMESS.[101]

TABLE I. Stationary points on the ground (S_0) PES of $BrC_\alpha H_2C(O)Cl$. Structures were optimized at the SS-CASSCF level and energies computed at the 6S-MC-QDPT level. (Energies are in eV relative to the *trans*-C_s min structure; geometries are in Å and deg. The MC-QDPT energy of ground-state *trans*-C_s min is $-3181.526\,739E_h$. Values in brackets are from experiment, with the experimental error bar, if available, in parentheses).

	cis-C_s TS1	*gauche* min	*gauche*-to-*trans* TS2	*trans*-C_s min[a]
R(C–Cl)	1.7984	1.8124	1.8210	1.824 [1.789(0.011)]
R(C–O)	1.1811	1.1794	1.1770	1.175 [1.188(0.009)]
<ClCO	121.3	122.0	121.7	121.8
R(C–C_α)	1.5174	1.5047	1.5093	1.505 [1.519(0.018)]
<C_αCO	119.8	125.1	125.9	129.3 [127.6(1.3)]
<C_αCOCl	180.0	−178.3	−177.8	180.0
R(C_α–Br)	1.9667	1.9858	1.9861	1.973 [1.935(0.012)]
<BrC_αC	119.5	110.5	110.1	112.4 [111.0(1.5)]
<BrC_αCCl	0.0	74.4	122.8	180.0
R(H_1–C_α)	1.0782	1.0763	1.0734	1.078 [1.086(0.062)]
<H_1C_αC	107.4	111.7	112.7	109.8
<H_1C_αCCl	58.6	−44.0	3.7	60.4
R(H_2–C_α)	1.0782	1.0769	1.0792	1.078 [1.086(0.062)]
<H_2C_αC	107.4	109.2	109.2	109.8
<H_2C_αCCl	−58.6	−168.6	−120.7	−60.4
Energy	0.13 [0.14[b]]	0.03 [0.05,[b] 0.04[c]]	0.08 [0.12[b]]	0.0 [0.0]

[a]Experimental structure taken from Ref. 102.
[b]Experimental data taken from Ref. 103.
[c]Experimental data taken from Ref. 104.

III. RESULTS

III.A. Ground-state (S_0) PES and dissociation products

The geometries of the stationary points (minima and saddle points) on the ground-state (S_0) PES and their energies were computed at the SS-CASSCF and 6S-MC-QDPT levels, respectively, and they are reported in Table I. The diagram in Fig. 1 illustrates the key pathways connecting these points and also shows the structure of the products and the dissociation energies. Two stable torsional isomers were found on the S_0 PES, with the isomer with a *trans* conformation of the halogen atoms being more stable than the structure with a *gauche* conformation. The geometrical parameters of the *trans* minimum are generally in good agreement with experiment,[102] with the largest discrepancy being observed for the C–Cl distance [1.82 Å at the SS-CASSCF level versus the experimental 1.79 Å (Ref. 102)]. The relative energies of the rotamers in the gas phase have been determined experimentally,[103,104] and Table I shows that the 6S-MC-QDPT values are in good agreement with experiment. Two interconversion transition states were also characterized, one connecting the *trans* and *gauche* conformers and the other connecting the two equivalent, mirror-image *gauche* and *gauche'* conformers (see Fig. 1). The heights of the torsional barriers have been estimated from experiment,[104] and those values are in reasonably good agreement with the 6S-MC-QDPT results (see Table I). We conclude that the combination of 6S-MC-QDPT energies with SS-CASSCF geometries provides a semiquantitative description of the S_0 PES in the region of the equilibrium structures. Since these state-averaged calculations treat the six lowest states evenhandedly (for a given Gaussian basis set), this is encouraging for their accuracy for the conformations of the excited states, where no such detailed experimental data are available.

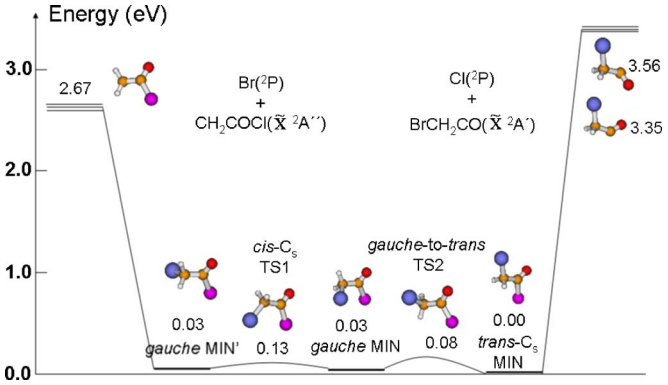

FIG. 1. Stationary points on the ground (S_0) PES of $BrC_\alpha H_2C(O)Cl$ and ground-state products of C–Cl and C_α–Br photodissociation. The products are shown as threefold degenerate because spin-orbit coupling is not included in this article. The structures shown are optimized at the SS-CASSCF level, and the energies shown are computed at the 6S-MC-QDPT level. Energies are given in eV relative to the energy of *trans*-C_s.

The structures and energies of the ground and first excited states of the product molecular fragments are presented in Table II. In the absence of detailed experimental or previous theoretical information for the chlorovinoxy radical [$C_\alpha H_2C(O)Cl$], a comparison can be made to the vinoxy radical (CH_2CHO).[105–109] The geometries of the ground ($\tilde{X}\,^2A''$) and first excited states ($\tilde{A}\,^2A'$) of vinoxy were optimized here at the SS-CASSCF(7,6)/6–31G(d,p) level, with an active space defined in analogy to that of $C_\alpha H_2C(O)Cl$, in particular, seven electrons in six orbitals. The results show reasonable agreement between the key C–C

TABLE II. Geometries and relative energies of the molecular fragments of the C–Cl and C_α–Br dissociations. Structures were optimized at the SS-CASSCF level and energies were computed at the 2S-MC-QDPT level based on a SA(2)-CASSCF reference function. (Geometries are given in Å and deg.)

	$C_\alpha H_2C(O)Cl$ $(\tilde{X}\,^2A'')$	$C_\alpha H_2C(O)Cl$ $(\tilde{A}\,^2A')$	$BrC_\alpha H_2CO$ *cis* $(\tilde{X}\,^2A')$	$BrC_\alpha H_2CO$ *gauche* $(\tilde{X}\,^2A)$	$BrC_\alpha H_2CO$ $(\tilde{A}\,^2A'')$
R(C–Cl)	1.8203	1.7590	⋯	⋯	⋯
R(C–O)	1.1886	1.3396	1.1751	1.1796	1.1878
<ClCO	121.0	109.0	⋯	⋯	⋯
R(C–C_α)	1.4462	1.3297	1.4911	1.5084	1.4576
<C_αCO	125.9	126.1	132.0	126.3	179.2
<C_αCOCl	180.0	180.0	⋯	⋯	⋯
R(C_α–Br)	⋯	⋯	2.0032	1.9846	1.9944
<BrC_αC	⋯	⋯	114.0	109.9	107.1
<BrC_αCO	⋯	⋯	0.0	133.9	180.0
R(H_1–C_α)	1.0719	1.0732	1.0786	1.0783	1.0820
<H_1C_αC	117.2	120.1	109.7	109.9	114.0
<H_1C_αCO	180.0	180.0	119.7	−109.8	63.8
R(H_2–C_α)	1.0688	1.0706	1.0786	1.0791	1.0820
<H_2C_αC	121.5	120.4	109.7	112.1	114.0
<H_2C_αCO	0.0	0.0	−119.7	14.5	−63.8
ΔE[a]	0.0	1.56	0.0	0.20	1.50
E[b]	2.67	4.23	3.35	3.56	4.86

[a]Relative energies in eV relative to the most stable minimum of the ground electronic state of each species.
[b]Energies in eV relative to the overall zero of energy of Table I.

and C–O bond lengths and experiment for the ground state (experimental values[107] in parentheses): R_{C-C}=1.439 Å (1.405 Å) and R_{C-O}=1.215 Å (1.272 Å). The $\tilde{X}$-$\tilde{A}$ adiabatic excitation energy of vinoxy was computed at the 2S-MC-QDPT level based on a SA-CASSCF(7,6)/6–31G(d,p) reference function with an equal weight for the $\tilde{X}$ and $\tilde{A}$ states. An excitation energy of 1.03 eV was obtained, in excellent agreement with experiment [0.99 eV (Ref. 110)]. As shown in Table II, for the chlorovinoxy radical [$C_\alpha H_2C(O)Cl$], the C–C and C–O bond distances (1.446 and 1.189 Å, respectively) and the adiabatic excitation energy to the first excited state (1.56 eV) are significantly different from those for the vinoxy radical. The good agreement between theory and experiment for the vinoxy radical gives us confidence that the theoretical description of the chlorovinoxy radical should also be accurate.

A comparison can also be made between the molecular product of the C–Cl fission, i.e., the bromoacetyl radical ($BrC_\alpha H_2CO$) and the well-studied acetyl (CH_3CO) radical. The most stable minimum on the ground state of the acetyl radical is bent with a CCO bending angle of about 128° and an eclipsed conformation of the CH_3 group,[108,111] in good agreement with the geometry of *cis*-bromoacetyl in Table II. For the excited $(\tilde{A}\,^2A'')$ state of $BrC_\alpha H_2CO$ the minimum restricted to C_s symmetry has a $C_\alpha CO$ bending angle of almost 180°. This structure is a transition state with a symmetry-breaking imaginary frequency, as in the case of the acetyl radical.[111] This transition state connects the two equivalent bent minima of the ground-state PES. An approximation to the adiabatic excitation energy for the $\tilde{A}$ state of CH_3CO was computed[111] using time-dependent density functional theory with the B3LYP functional (TD-B3LYP) by optimizing the ground-state geometry at the B3LYP level for several values of the C–C–O bending coordinate and subsequent single-point excited state-energy calculations. The excitation energy obtained was around 1 eV,[111] which is lower than the adiabatic excitation energy calculated here for $BrC_\alpha H_2CO$ (1.51 eV). For the sake of comparison, the geometries of the ground $(\tilde{X}\,^2A')$ and first excited state $(\tilde{A}\,^2A'')$ of CH_3CO were optimized here at the SS-CASSCF(7,6)/6–31G(d,p) level, with an active space defined in analogy to that of $BrC_\alpha H_2CO$. The adiabatic excitation energy was computed at the 2S-MC-QDPT level based on a SA-CASSCF(7,6)/6–31G(d,p) reference function with an equal weight for the $\tilde{X}$ and $\tilde{A}$ states. A value of 1.32 eV was obtained, somewhat larger than the approximate excitation energy obtained at the TD-B3LYP level (about 1 eV).[111]

The C–Cl and C_α–Br dissociation energies from the *trans*-C_s minimum of $BrC_\alpha H_2C(O)Cl$ on the S_0 PES to products in their ground and first excited electronic states are presented in Table III. The 6S-MC-QDPT results are compared with those obtained at the RCCSD(T)/IB level and with experimental bond dissociation energies. Since experimental bond energies for bromoacetyl chloride are not available, it seems appropriate to compare the C_α–Br dissociation energy with that of a system like allyl bromide ($BrCH_2CHCH_2$), which shows an analogous stabilization by resonance in the product allyl radical as for the chlorovinoxy radical. As seen in Table III, for the C_α–Br bond rupture the 6S-MC-QDPT method underestimates the experimental dissociation energy of allyl bromide[112] by about 0.2 eV, while the RCCSD(T)/IB results are in good agreement with experiment. For the C–Cl dissociation, 6S-MC-QDPT shows a deviation from the experimental bond energy of acetyl chloride

TABLE III. Dissociation energies from *trans*-C_s min on the S_0 PES to products. [Energies in eV. The ground-state classical dissociation energies (D_e) are corrected by adding the SS-CASSCF zero-point energy (ZPE) difference between $BrC_\alpha H_2C(O)Cl$ and products and −1/3 times the experimental SO energy splitting between the $^2P_{3/2}$ and $^2P_{1/2}$ states of the halogens.]

	$Br(^2P)+$ $C_\alpha H_2C(O)Cl(\tilde{X}\,^2A'')$	$Br(^2P)+$ $C_\alpha H_2C(O)Cl(\tilde{A}\,^2A')$	$Cl(^2P)+$ *cis*-$BrC_\alpha H_2CO(\tilde{X}\,^2A')$	$Cl(^2P)+$ $BrC_\alpha H_2CO(\tilde{A}\,^2A'')$
6S-MC-QDPT	D_e=2.67 D_0 with SO=2.38(1)[a]	D_e=4.23	D_e=3.35 D_0 with SO=3.21(1)[a]	D_e=4.86
RCCDS (T)/IB[b]	D_e=2.90 D_0 with SO=2.61	D_e=4.34	D_e=3.59 D_0 with SO=3.45	D_e=5.02
Experimental	$\Delta H_{298\ K}$=2.56±0.04 (for $BrCH_2CHCH_2$)[c]		D_0=3.60±0.04 (for CH_3COCl)[d]	

[a]The zero-point energies computed at the SS-CASSCF level are *trans*-min S_0: 1.11; $C_\alpha H_2C(O)Cl(\tilde{X}\,^2A'')$: 0.96; and *cis*-$BrC_\alpha H_2CO(\tilde{X}\,^2A')$: 1.01. The experimental SO splittings are 0.46 for the Br atom and 0.11 for the Cl atom as taken from Ref. 76.
[b]Energies calculated at optimal SS-CASSCF structures.
[c]Taken from Ref. 112.
[d]Taken from Ref. 113.

of about 0.4 eV, while the RCCSD(T)/IB energy differs by only 0.15 eV from experiment.[113] It is remarkable that for basis sets of comparable (double-zeta plus polarization) quality, the 6S-MC-QDPT method shows an accuracy comparable to the RCCSD(T) method, and both methods predict the dissociation energies with relative errors of about 10%. Hence, the largest part of the difference between the 6S-MC-QDPT and the experimental dissociation energies is due to limitations of the basis set employed.

III.B. Adiabatic excited-state (S_1) PES

The calculated geometries of the stationary points found on the S_1 PES are presented in Table IV. Diagrams of the different structures and their relative energies at the 6S-MC-QDPT level are shown in Figs. 2 and 3. It is useful to distinguish the region of the minima and their interconversion transition states (which will be denoted region I, spanning columns 2–9 in Table IV and represented in the central region of Fig. 2 and in Fig. 3) from the regions of the transition states for the bond ruptures (regions II and III; columns 10–13 in Table IV and rightmost and leftmost regions of Fig. 2). As will be discussed in the last paragraph of this section, none of these three regions is in the Franck-Condon region for excitation from S_0.

Region I is the bound region of the adiabatic S_1 PES. The most remarkable differences between the strong interaction region of S_0 and region I of the S_1 PES are the C–O bond length and the C_α–C–O–Cl dihedral angle. There is an increase in the C–O bond length from about 1.18 Å for the S_0 PES to 1.34–1.35 Å for the S_1 PES, and the groups linked to the carbonyl C atom in the S_1 state adopt a pyramidal conformation, as evidenced by the values of the C_α–C–O–Cl dihedral angle (135°–145°) in Table IV. These differences are due to the change in hybridization of the carbonyl C atom from nominally sp^2 in the ground state to nominally sp^3 in the excited state, which can be understood from the character of the excitation from S_0 to S_1 [$n(O) \rightarrow \pi^*(C{=}O)$].

TABLE IV. Stationary point geometries on the S_1 PES optimized at the SS-CASSCF level. (Units are Å and deg.)

	3-1 TS9	min3	2-3 TS8	min2	1-2 TS7	min1	*cis*-C_s TS11	*trans*-C_s TS10	C–Cl TS5	C–Cl TS4	C–Cl TS3	C–Br TS6
R(C–Cl)	1.766	1.773	1.760	1.760	1.778	1.780	1.735	1.747	2.122	2.117	2.120	1.745
R(C–O)	1.348	1.345	1.351	1.342	1.342	1.344	1.357	1.351	1.248	1.243	1.251	1.331
<ClCO	110.4	109.1	109.2	110.6	108.9	108.9	113.3	113.5	97.8	98.4	98.4	110.8
R(C–C_α)	1.487	1.499	1.509	1.464	1.506	1.493	1.490	1.487	1.504	1.478	1.497	1.389
<C_αCO	116.6	113.4	112.8	118.6	119.0	116.7	116.7	125.0	123.5	129.5	125.9	123.5
<C_αCOCl	140.7	134.0	142.1	145.2	137.3	132.7	180.0	180.0	117.2	123.4	114.4	166.1
R(C_α–Br)	2.011	1.987	1.983	2.046	1.993	1.994	1.978	1.989	1.979	2.017	1.994	2.336
<BrC_αC	110.8	111.5	116.2	112.5	112.9	110.1	113.7	111.3	111.6	114.0	109.1	108.4
<BrC_αCCl	−109.0	−70.8	−4.7	73.7	138.0	−167.9	0.0	180.0	−73.6	73.6	−169.3	84.8
R(H_1–C_α)	1.078	1.079	1.078	1.076	1.078	1.080	1.080	1.081	1.079	1.075	1.079	1.071
<H_1C_αC	111.4	109.9	110.1	111.6	111.5	112.0	110.9	112.0	108.6	111.0	111.8	116.5
<H_1C_αCCl	134.3	171.7	−123.7	−44.4	18.6	74.4	119.2	61.8	169.5	−46.9	73.4	−24.5
R(H_2–C_α)	1.076	1.079	1.080	1.078	1.078	1.076	1.080	1.081	1.078	1.078	1.075	1.073
<H_2C_αC	112.8	112.1	109.7	111.4	110.7	110.8	110.9	112.0	112.3	109.4	110.9	116.2
<H_2C_αCCl	8.6	48.5	115.2	−169.9	−104.3	−50.4	−119.2	−61.8	46.8	−169.7	−52.2	−167.8

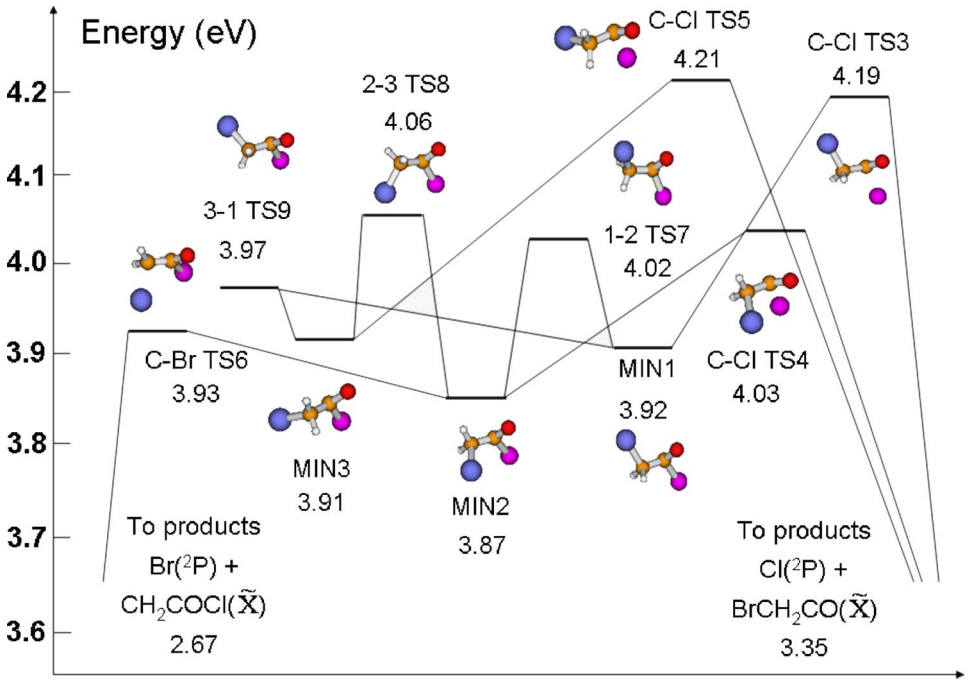

FIG. 2. Stationary points on the first excited (S_1) PES of $BrC_\alpha H_2C(O)Cl$. Structures are optimized at the SS-CASSCF level and energies computed at the 6S-MC-QDPT level. Energies are given in eV relative to the S_0 energy of the *trans*-C_s structure.

The bound region of the S_0 PES strongly resembles region I of the S_1 PES. In both cases there are three different rotational isomers that differ in the value of the $Br-C_\alpha-C-Cl$ dihedral angle (see Figs. 1 and 2) and in the $H-C_\alpha-C-Cl$ dihedral angles, because the $-BrC_\alpha H_2$ group executes an essentially rigid torsion around the carbon-carbon bond. min1 is analogous to the *trans*-C_s minimum, and min2 and min3 are analogous to the two *gauche* minima on the S_0 PES (e.g., compare the $Br-C_\alpha-C-Cl$ dihedral angles in Tables I and IV). Furthermore, the 6S-MC-QDPT relative stabilities of the minima are quite comparable, as are the barrier heights of the interconversion transition states: a smaller barrier of about 0.1 eV for the *trans-gauche* conversion on S_0 (Fig. 1) and the min1-min2 and min3-min1 conversions on S_1 (Fig. 2), and a larger barrier of 0.15–0.20 eV for the *gauche-gauche'* (S_0) and the min2-min3 conversions

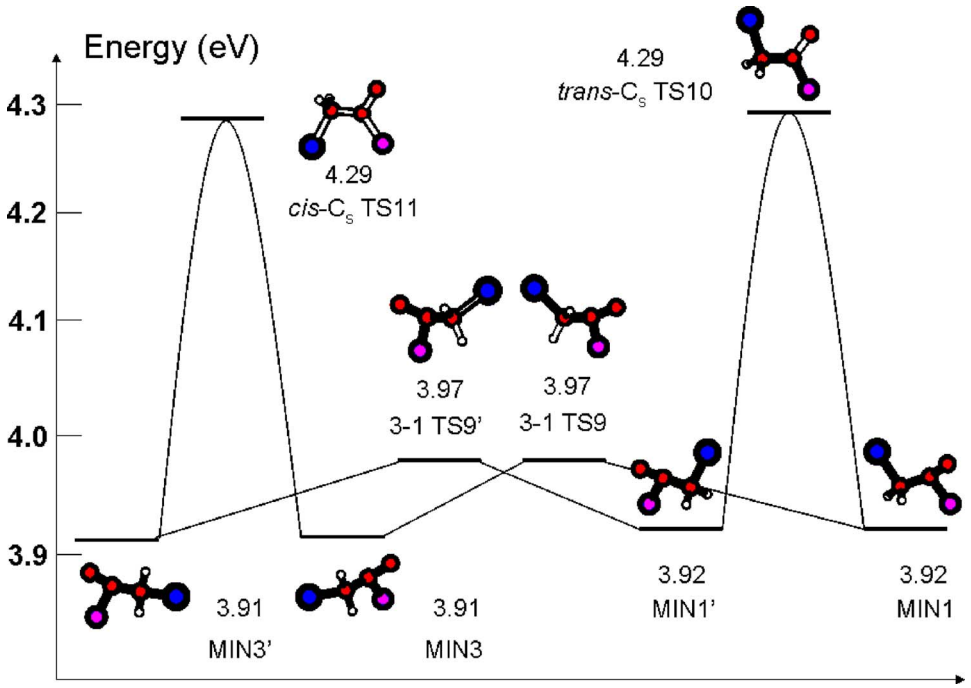

FIG. 3. Equivalent minima and interconversion transition states on the S_1 PES. Structures are optimized at the SS-CASSCF level and energies computed at the 6S-MC-QDPT level. Energies are given in eV relative to the S_0 energy of the *trans*-C_s structure.

TABLE V. Diabatic group lists for the five diabatic states of $BrC_\alpha H_2C(O)Cl$. [p_π and p'_π represent nonbonding orbitals and p_σ a bonding orbital of the halogen atoms for short values of the C_α–Br and C–Cl bond distances. π is mainly a π(C=O) DMO; n(O) is a nonbonding DMO centered on the oxygen atom; u^* and v^* are DMOs that are mainly a combination of π^*(C=O) and σ^*(C–Cl); w^* is mainly a combination of π^*(C=O) and $\sigma^*(C_\alpha$–Br).]

Group 2	χ_1: $p_\sigma(\mathrm{Cl})^1 p_\sigma(\mathrm{Br})^2 p_\pi(\mathrm{Cl})^2 p'_\pi(\mathrm{Cl})^2 p_\pi(\mathrm{Br})^2 p'_\pi(\mathrm{Br})^2 \pi^2 n(\mathrm{O})^2 u^{*1} v^{*0} w^{*0}$
	χ_2: $p_\sigma(\mathrm{Cl})^2 p_\sigma(\mathrm{Br})^2 p_\pi(\mathrm{Cl})^2 p'_\pi(\mathrm{Cl})^2 p_\pi(\mathrm{Br})^2 p'_\pi(\mathrm{Br})^2 \pi^2 n(\mathrm{O})^1 u^{*0} v^{*0} w^{*1}$
	χ_3: $p_\sigma(\mathrm{Cl})^2 p_\sigma(\mathrm{Br})^1 p_\pi(\mathrm{Cl})^2 p'_\pi(\mathrm{Cl})^2 p_\pi(\mathrm{Br})^2 p'_\pi(\mathrm{Br})^2 \pi^2 n(\mathrm{O})^1 u^{*2} v^{*0} w^{*0}$
	χ_4: $p_\sigma(\mathrm{Cl})^2 p_\sigma(\mathrm{Br})^1 p_\pi(\mathrm{Cl})^2 p'_\pi(\mathrm{Cl})^2 p_\pi(\mathrm{Br})^2 p'_\pi(\mathrm{Br})^2 \pi^2 n(\mathrm{O})^1 u^{*1} v^{*0} w^{*1}$
Group 3	χ_5: $p_\sigma(\mathrm{Cl})^2 p_\sigma(\mathrm{Br})^2 p_\pi(\mathrm{Cl})^2 p'_\pi(\mathrm{Cl})^1 p_\pi(\mathrm{Br})^2 p'_\pi(\mathrm{Br})^2 \pi^2 n(\mathrm{O})^2 u^{*1} v^{*0} w^{*0}$
	χ_6: $p_\sigma(\mathrm{Cl})^2 p_\sigma(\mathrm{Br})^2 p_\pi(\mathrm{Cl})^2 p'_\pi(\mathrm{Cl})^2 p_\pi(\mathrm{Br})^1 p'_\pi(\mathrm{Br})^2 \pi^2 n(\mathrm{O})^1 u^{*2} v^{*0} w^{*0}$
	χ_7: $p_\sigma(\mathrm{Cl})^2 p_\sigma(\mathrm{Br})^2 p_\pi(\mathrm{Cl})^2 p'_\pi(\mathrm{Cl})^2 p_\pi(\mathrm{Br})^1 p'_\pi(\mathrm{Br})^2 \pi^2 n(\mathrm{O})^1 u^{*1} v^{*0} w^{*1}$
	χ_8: $p_\sigma(\mathrm{Cl})^2 p_\sigma(\mathrm{Br})^2 p_\pi(\mathrm{Cl})^2 p'_\pi(\mathrm{Cl})^2 p_\pi(\mathrm{Br})^2 p'_\pi(\mathrm{Br})^2 \pi^1 n(\mathrm{O})^2 u^{*1} v^{*0} w^{*0}$
Group 4	χ_9: $p_\sigma(\mathrm{Cl})^2 p_\sigma(\mathrm{Br})^2 p_\pi(\mathrm{Cl})^1 p'_\pi(\mathrm{Cl})^2 p_\pi(\mathrm{Br})^2 p'_\pi(\mathrm{Br})^2 \pi^2 n(\mathrm{O})^2 u^{*1} v^{*0} w^{*0}$
	χ_{10}: $p_\sigma(\mathrm{Cl})^2 p_\sigma(\mathrm{Br})^2 p_\pi(\mathrm{Cl})^2 p'_\pi(\mathrm{Cl})^2 p_\pi(\mathrm{Br})^2 p'_\pi(\mathrm{Br})^1 \pi^2 n(\mathrm{O})^1 u^{*2} v^{*0} w^{*0}$
	χ_{11}: $p_\sigma(\mathrm{Cl})^2 p_\sigma(\mathrm{Br})^2 p_\pi(\mathrm{Cl})^2 p'_\pi(\mathrm{Cl})^1 p_\pi(\mathrm{Br})^2 p'_\pi(\mathrm{Br})^1 \pi^2 n(\mathrm{O})^1 u^{*1} v^{*0} w^{*1}$
Group 5	χ_{12}: $p_\sigma(\mathrm{Cl})^2 p_\sigma(\mathrm{Br})^2 p_\pi(\mathrm{Cl})^2 p'_\pi(\mathrm{Cl})^1 p_\pi(\mathrm{Br})^2 p'_\pi(\mathrm{Br})^2 \pi^2 n(\mathrm{O})^2 u^{*0} v^{*1} w^{*0}$
	χ_{13}: $p_\sigma(\mathrm{Cl})^2 p_\sigma(\mathrm{Br})^2 p_\pi(\mathrm{Cl})^2 p'_\pi(\mathrm{Cl})^2 p_\pi(\mathrm{Br})^2 p'_\pi(\mathrm{Br})^1 \pi^2 n(\mathrm{O})^2 u^{*0} v^{*0} w^{*1}$
Group 6	χ_{14}: $p_\sigma(\mathrm{Cl})^2 p_\sigma(\mathrm{Br})^2 p_\pi(\mathrm{Cl})^1 p'_\pi(\mathrm{Cl})^2 p_\pi(\mathrm{Br})^2 p'_\pi(\mathrm{Br})^2 \pi^2 n(\mathrm{O})^2 u^{*0} v^{*1} w^{*0}$
	χ_{15}: $p_\sigma(\mathrm{Cl})^2 p_\sigma(\mathrm{Br})^2 p_\pi(\mathrm{Cl})^2 p'_\pi(\mathrm{Cl})^2 p_\pi(\mathrm{Br})^1 p'_\pi(\mathrm{Br})^2 \pi^2 n(\mathrm{O})^2 u^{*0} v^{*0} w^{*1}$

(S_1). (These energies are relative to the absolute minima on each PES.) As shown in Fig. 3, there are two other transition states at higher energies on the S_1 PES, *trans*-C_s TS10 connecting the two equivalent min1 and min1′ minima and *cis*-C_s TS11 connecting the two equivalent min3 and min3′ minima. The similarity between the bound region of the S_0 PES and region I of the S_1 PES suggests that the geometries and relative energies of the stationary points of region I should be quite accurate, as was found above for the S_0 PES.

Regions II and III of the adiabatic S_1 PES are the exit channel regions with the bond rupture transition states. As shown in Fig. 2, there are three different transition states for the respective C–Cl bond scissions from the three minima on S_1 (i.e., C–Cl TS3, TS4, and TS5) and one transition state for C_α–Br scission (i.e., C–Br TS6). Table IV shows that the C–Cl distances computed at the SS-CASSCF level are almost the same for the three C–Cl transition states (close to 2.1 Å), as are the rest of the geometrical parameters except the dihedral angles related to torsion of the $-BrCH_2$ group. The transition state for C_α–Br scission shows a strong elongation of the C_α–Br bond and an almost planar conformation of the $C_\alpha H_2C(O)Cl$ moiety. Note the shortening of the C–O bond and especially the C_α–C bond, relative to those typical of region I. The similarity between the values of these bond lengths in C–Br TS6 and the ones of $C_\alpha H_2C(O)Cl$ in its excited state (see Table II) suggests that C–Br TS6 has its major contribution from the bound diabatic electronic wave function. The lowest adiabatic barriers to dissociation connect the absolute minimum on the S_1 PES (min2) to products in their ground state.

The excitation energies from the S_0 PES to the S_1 PES in the Franck-Condon region are also relevant to the reaction dynamics. The MC-QDPT calculations predict that the excited state is not accessible to vertical excitation from the lowest-energy (*trans*-C_s) minimum on the S_0 PES: the 6S-MC-QDPT excitation energy is 5.37 eV, higher than the energy provided by the laser in the experiments (5.00 eV). The 2S-MC-QDPT excitation energy is slightly higher, namely, 5.44 eV. This is contrary to the assumption made in all previous studies that the excitation to S_1 is at the geometry of the *trans*-C_s conformer on S_0.[31–33,36,46–48] In fact, the prediction that excitation from the *trans* conformer is not energetically feasible is made not only by the older CIS calculations[33,36] but also by MRCI calculations[52] and by the present CASSCF and MC-QDPT calculations. Therefore, the *gauche* conformer must be considered for the Franck-Condon process. The MC-QDPT calculations predict that the S_1 PES is accessible at the geometry of the *gauche* conformer, with an excitation energy about 0.5–0.6 eV lower than for the *trans*-C_s conformer. In particular, the 6S-MC-QDPT excitation energy is 4.81 eV whereas the 2S-MC-QDPT value is 4.99 eV.

III.C. Adiabatic (S_0-S_5) and diabatic (S_1-S_5) potential energy curves

The SA(6)-CASSCF energies of the lowest six adiabatic singlet states have been computed for the Br–C_α–C–Cl torsion angle with the rest of the coordinates fixed and for linear-synchronous-transit/bond stretch pathways along the PESs involving mainly the C–Cl and C_α–Br dissociation coordinates. As explained in Sec. II.D, the five highest adiabatic states were transformed by the fourfold way to a diabatic potential matrix containing the diabatic PESs and couplings, while the ground state is assumed to remain adiabatic.

Adiabatic energies and diabatic potential energies and couplings were first computed for torsional potential curves around the geometry of min1, but with the C_α–C–O–Cl dihedral angle set to 180° and varying only the Br–C_α–C–Cl dihedral angle. When both the C_α–C–O–Cl

and Br–C_α–C–Cl dihedral angles are equal to either 0° or 180°, the $BrC_\alpha H_2C(O)Cl$ molecule contains a plane of symmetry; this causes some of the diabatic couplings to be zero by symmetry for these particular configurations.

Table V gives the diabatic group lists for diabatic states 2–6. The diabatic groups (states) are numbered following their energetic ordering, and the geometry corresponds to min1 except that the C_α–C–O–Cl dihedral angle is set to 180°; note that diabatic state 1 is the same as the adiabatic ground state. The nomenclature of the DMOs in the table corresponds to a general nonsymmetrical structure with mixing between orbitals that are, for instance, of σ^* and π^* characters at symmetric geometries. The mixing is strongly dependent on the C_α–Br and C–Cl distances, especially for the virtual DMOs, as was explained in Sec. II.C. This is due to the improved flexibility of the fourfold way over previous diabatization methods. Thus, the fourfold way allows different DCSFs in a given diabatic group to be dominant in different geometric regions.[26,53,54] One consequence is that the character of some of the DMOs must change along the reaction coordinate, but since they do so in a smooth way they provide proper diabatic states and energies for the process or processes under consideration. Note that when the molecule has a plane of symmetry, all CSFs with nonzero coefficients in a given group have the same symmetry. For instance, for the geometry of min1 but with the Br–C_α–C–Cl and C_α–C–O–Cl dihedral angles both equal to 180°, the CSFs with nonzero coefficients are (see Table V) $\chi_2(^1A'')$, χ_5 and $\chi_8(^1A')$, and $\chi_9(^1A'')$, $\chi_{13}(^1A'')$, and $\chi_{15}(^1A')$, for groups 2–6, respectively. For this particular geometry, all DMOs are either of a' or a'' symmetry; the ones that determine the symmetry of the dominant CSFs in each group are as follows: n(O) (a') and $w^* \equiv \pi^*$(C═O) (a'') for group 2; p'_π(Cl) (a''), π(C═O) (a''), and $u^* \equiv \pi^*$(C═O) (a'') for group 3; p_π(Cl) (a') and $u^* \equiv \pi^*$(C═O) (a'') for group 4; p'_π(Br) (a'') and $w^* \equiv \sigma^*(C_\alpha\text{–Br})$ (a') for group 5; and p_π(Br) (a') and $w^* \equiv \sigma^*(C_\alpha\text{–Br})$ (a') for group 6.

The diabatic couplings for the Br–C_α–C–Cl torsional curves are presented in Fig. 4. We chose this particular coordinate (the Br–C_α–C–Cl dihedral angle) to illustrate the couplings because this is the coordinate that differs the most between the stationary points on the S_1 PES (see Table IV). The symmetries of the diabatic states determine that the (23), (26), (34), (35), (46), and (56) diabatic couplings must be zero. As shown in Fig. 4, the (23), (34), (26), and (56) couplings vanish when the Br–C_α–C–Cl dihedral angle is 0° and 180°; the (26) and (46) couplings also vanish at these geometries (not shown). The signs of the diabatic couplings presented in Fig. 4 are chosen arbitrarily but consistently with the signs in the other regions of the PESs (see Secs. II.B and II.C). Points with suitable values of the Br–C_α–C–Cl dihedral angle are picked from the torsional curve and are connected to the minima on the S_1 PES (min1, min2, and min3) by pathways composed of two segments: (1) In the first segment only C–Cl and C_α–Br are stretched to attain a region of bond distances where the diabatic couplings keep their signs; (2) the second segment is a linear-synchronous-transit/bond stretch pathway starting at the last point of segment 1 and in which the main change is in the C_α–C–O–Cl

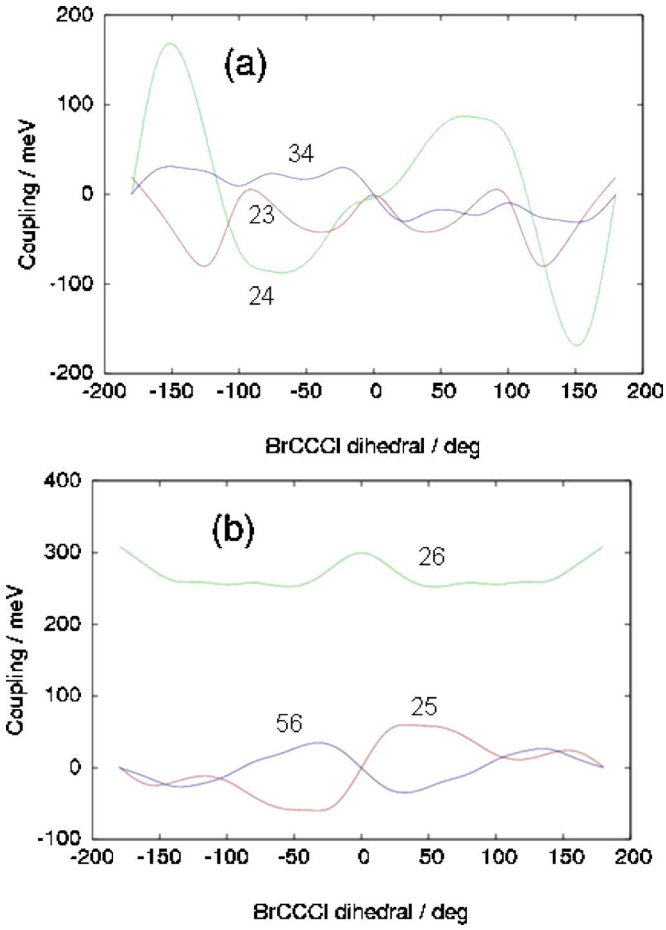

FIG. 4. Diabatic couplings computed along the Br–C_α–C–Cl torsional coordinate for min1 but with a C_α–C–O–Cl dihedral angle of 180° (see Sec. III.C) at the SA(6)-CASSCF level. All other coordinates are fixed at the values presented in Table IV. Couplings relevant to C_α–Br dissociation are shown in panel (a) and those relevant to C–Cl dissociation in panel (b). The torsional angle is defined as 180° for the *trans* conformation.

dihedral angle (i.e., the carbonyl carbon relaxes to its minimal energy configuration). From the minima, either simple stretching of the C–Cl and C_α–Br coordinates or linear-synchronous-transit/bond stretching pathways connecting with the different transition states and with products can be constructed. This procedure allows one to define consistently the signs of the diabatic couplings in the relevant region of configuration space.

Panel (a) of Fig. 5 presents adiabatic potential energy curves along the C–Cl and C_α–Br coordinates for the lowest six adiabatic singlet states starting at the geometry of *trans*-C_s TS10, but with Br–C_α–C–Cl set to 170°. Although the actual minimum energy path does not involve dissociation directly from *trans*-C_s TS10, these hypothetical dissociation pathways are constructed for the sake of comparison with previous studies. In particular, two adiabatic electronic state intersections of the second adiabatic state (S_1) with the third and fourth adiabatic states (S_2 and S_3) are observed for stretched values of the C_α–Br (left) and C–Cl (right) bonds. This is different from what has been assumed in all previous studies, i.e., that the dynamics proceeds keeping a plane of molecular symmetry and that only two electronic states of $^1A''$ symmetry participate in the avoided crossings in the

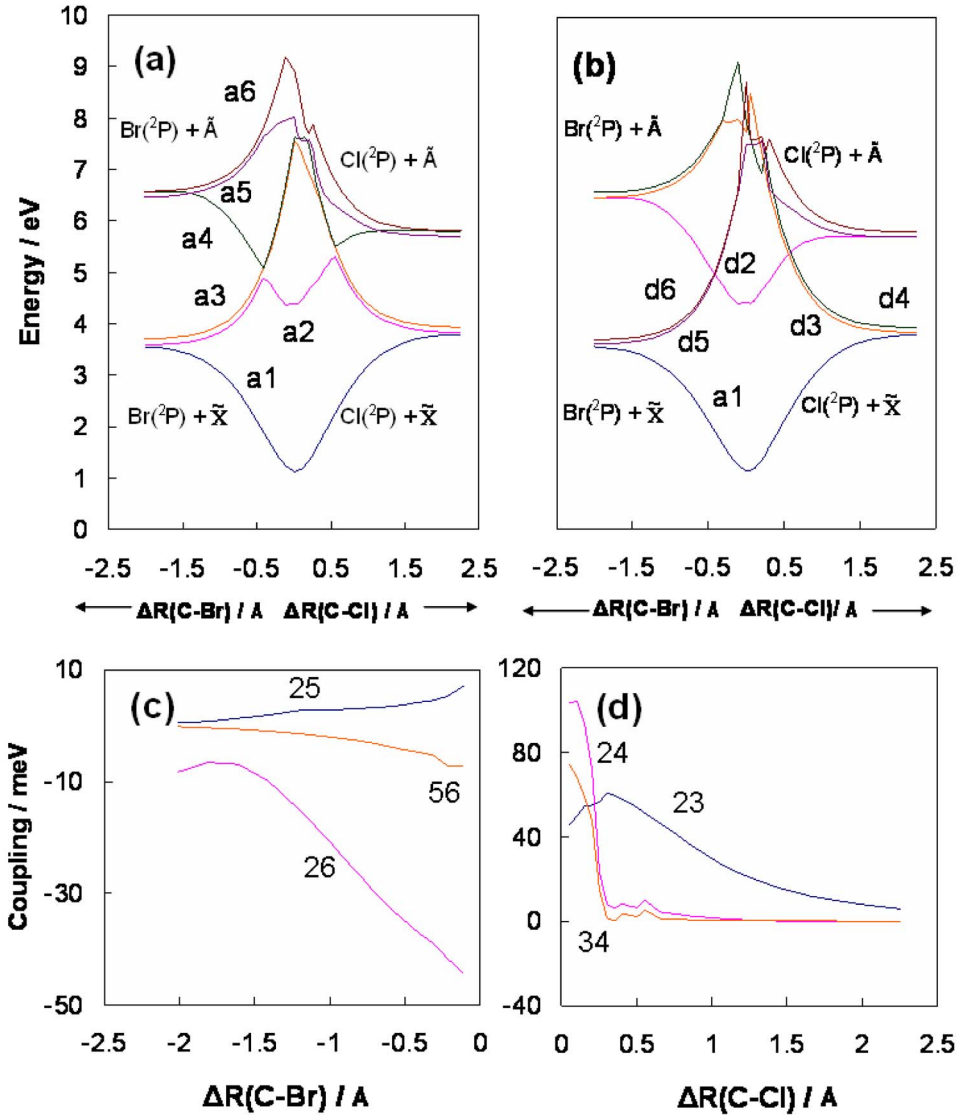

FIG. 5. Potential energy curves and diabatic couplings along the C–Cl and C_α–Br dissociation coordinates at the SA(6)-CASSCF level. The geometries are the same as those for *trans*-C_s TS10 (see Fig. 3 and Table IV) but with a Br–C_α–C–Cl dihedral angle of 170° (see text), and the C–Cl and C_α–Br bond distances are varied. The abscissa values are referenced to the respective equilibrium distances of *trans*-C_s TS10, i.e., $\Delta R(C_\alpha\text{–Br}) \equiv 1.973$ Å $-R(C_\alpha\text{–Br})$ and $\Delta R(\text{C–Cl}) \equiv R(\text{C–Cl}) - 1.824$ Å. (a) Adiabatic energies, (b) adiabatic ground state and excited diabatic states, (c) diabatic couplings along the C_α–Br coordinate, and (d) diabatic couplings along the C–Cl coordinate. In Figs. 5, 6, and 9 Br denotes Br(^2P), $\tilde{X}$ denotes the ground state of $CH_2C(O)Cl$ or CH_2BrCO, and $\tilde{A}$ denotes the first excited state of $CH_2C(O)Cl$ or CH_2BrCO.

C–Cl and C_α–Br exit channels.[32,33,36,46–48] Spin-orbit coupling (which is neglected here) will split the two transition states but we have not calculated by how much. The SA(6)-CASSCF energies predict that passing over the barrier for the C–Cl dissociation is not energetically feasible at 5 eV of total energy, while the barrier to C_α–Br dissociation is barely accessible. Furthermore, for the system to evolve toward *trans*-C_s TS10, (a) the excitation energy at the Franck-Condon geometry of *trans*-C_s min should be less than 5 eV and (b) the system should keep a plane of symmetry, as assumed in previous studies. However, given that the S_1 state is inaccessible or barely accessible at the geometry of *trans*-C_s min (see above), that the system is likely to distort away from structures with a plane of symmetry after excitation from the S_0 state, and because of the large barriers to dissociation from *trans*-C_s TS10, it is unlikely that the reaction proceeds along this pathway. Note the complicated pattern of curve crossings starting at about 6 eV and involving the highest four adiabatic states.

In panel (b) of Fig. 5 the diabatic energies of the first five excited states along with the adiabatic ground-state energies are presented. One can see that the diabatic state corresponding to S_1 is essentially parallel to the adiabatic ground state (see Sec. III.B), while the diabatic states corresponding locally to S_2 and S_3 are repulsive in the C–X coordinate and always remain almost degenerate. The behavior of the diabatic states for energies higher than about 6.5 eV is irregular; as a compromise, we allowed the diabatic states in this region to be nonsmooth in order to obtain the simplest globally correct diabatization in the energetically allowed regions of the PESs (see Sec. II.C).

Panels (c) and (d) of Fig. 5 show the diabatic couplings for the three lowest diabats that intersect along the C_α–Br and C–Cl coordinates, respectively. The other diabatic couplings are ignored because rediagonalization of the diabatic Hamiltonian with only three couplings in region II [(25), (26), and (56)] and three couplings [(23), (24), and (34)] in region III affords a good reproduction of the adiabatic energies of S_1, S_2, and S_3. The magnitude of the largest off-diagonal element of the diabatic potential matrix at the geometry of the intersections is 300 cm^{-1} (37 meV) for the (26) element along the C_α–Br coordinate and 400 cm^{-1} (50 meV) for the (23) off-diagonal element along the C–Cl coordinate. The other couplings are much smaller, as seen in

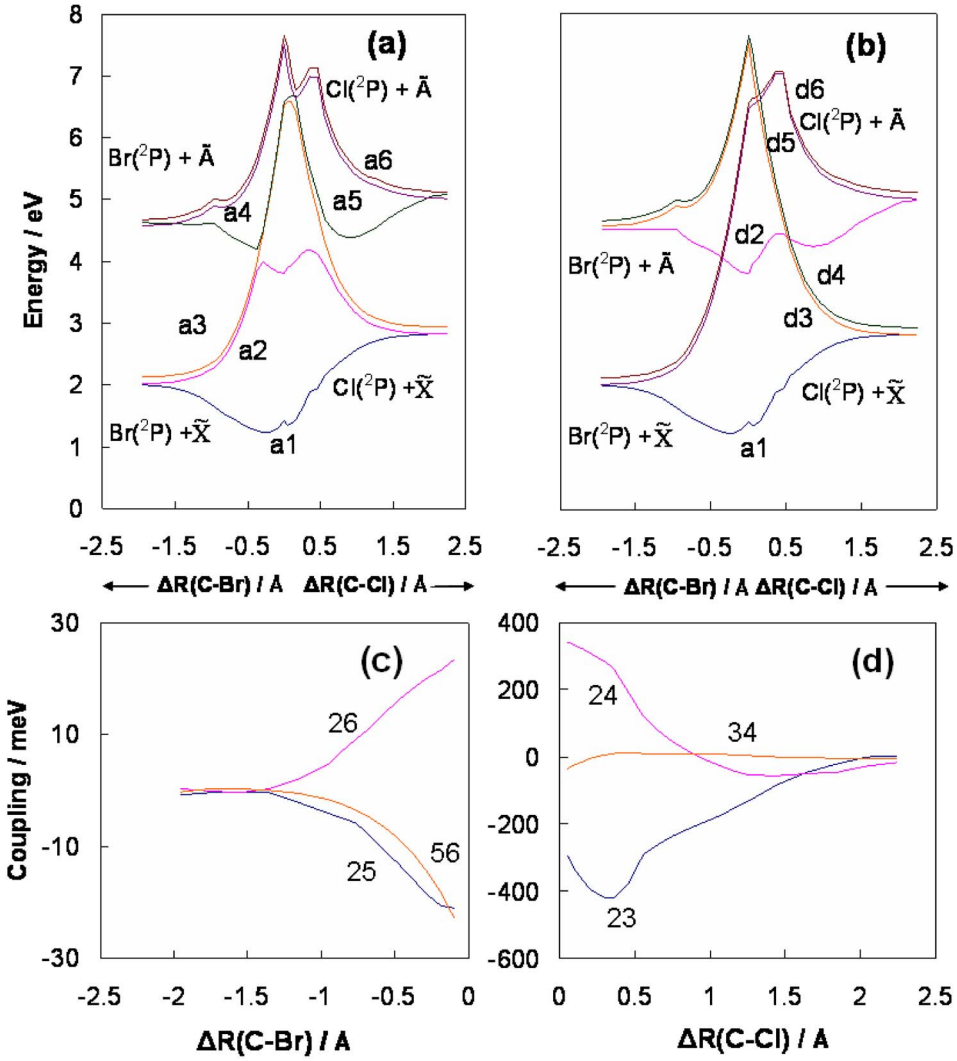

FIG. 6. Potential energy curves and diabatic couplings along the C–Cl and C_α–Br dissociation coordinates for linear-synchronous-transit/bond stretch paths from min2 through C–Cl TS4 and C–Br TS6 and then out to C–Cl and C_α–Br bond distances of about 3 Å, respectively, as described in the second last paragraph of Sec. II.D. Note that for bond distances between 3 and 4 Å, the bonds were stretched keeping the other coordinates fixed. Energies were computed at the SA(6)-CASSCF level. The C–Cl and C_α–Br bond distances are referenced to the respective equilibrium distances of min2. The values of the other coordinates are as shown for structure min2 in Table IV.

the figure. Other authors have reported only one diabatic coupling between two electronic states at planar geometries. Lasorne *et al.* assumed constant diabatic couplings in their 2D wave packet calculations, in which the dynamics was propagated starting at the equilibrium geometry of *trans*-C_s TS10.[47] The values assumed by the authors, 160 cm^{-1} (20 meV) for C_α–Br and 360 cm^{-1} (45 meV) for C–Cl, are in qualitative agreement with those obtained here at the SA(6)-CASSCF level in the vicinity of the diabatic curve crossings, but the present values vary with geometry. Kash *et al.*[33] computed diabatic couplings in the range of 34–112 cm^{-1} (4–14 meV) for the C_α–Br coordinate and in the range of 27–580 cm^{-1} (3–72 meV) for the C–Cl coordinate as a function of the C–O bond distance. At C–O distances comparable to the one of *trans*-C_s TS10, they reported very low couplings and a smaller splitting at the C–Cl barrier than at the C_α–Br barrier. Their values are in general lower than those obtained here.

Figure 6 represents linear-synchronous-transit/bond stretch pathways connecting min2, the absolute minimum on the adiabatic S_1 PES, with the lowest adiabatic barriers (formed by C–Br TS6 and C–Cl TS4) and with products. These pathways should be a good approximation to the actual minimum energy path (MEP) after relaxation from the Franck-Condon region (see below). The adiabatic energies in panel (a) show the same qualitative behavior as those shown in Fig. 5. There are some irregularities in the ground-state adiabat, probably caused indirectly by the spikes observed in the energies of the sixth adiabatic state. This is not relevant, since the only portion of the S_0 PES required to simulate the branching ratio in the photodissociation experiments is that near the minimum. All four dissociation channels in panel (a) are energetically accessible, except perhaps the $Cl(^2P)$ $+BrC_\alpha H_2CO(\tilde{A})$ channel which is close to the 5 eV limit. This is in qualitative agreement with the information presented in Table III, which corresponds to fully optimized product fragments. The magnitude of the diabatic couplings at the distances where diabatic states 2, 5, and 6 intersect is very small for the C_α–Br coordinate, only 150, 130, and 90 cm^{-1} (19, 16, and 11 meV) for the (25), (26), and (56) off-diagonal couplings, respectively. For the C–Cl dissociation, the (23), (24), and (34) couplings are 2300, 960, and 80 cm^{-1} (285, 119, and 10 meV), respectively. Note the difference from the couplings obtained above for *trans*-C_s TS10, pointing out the strong dependence of the diabatic couplings on the molecular structure. Thus, the C–Cl diabatic couplings are an order of magnitude larger than the C_α–Br

TABLE VI. Diabatic couplings (cm^{-1}) at all the transition states on the S_1 PES (8065 cm^{-1}=1 eV).

Diabatic coupling	C–Br TS6	C–Cl TS3	C–Cl TS4	C–Cl TS5	1-2 TS7	2-3 TS8	3-1 TS9	*cis*-C_sTS11	*trans*-C_sTS10
(23)	220	2300	3300	3070	2570	2040	2480	150	1140
(24)	810	960	2130	1230	2740	2600	2405	5	970
(34)	65	80	80	370	370	450	305	160	1950
(25)	150	310	480	80	280	880	120	20	60
(26)	130	830	240	720	1360	505	680	200	440
(56)	90	350	100	590	150	205	115	5	80

couplings at the avoided crossings. The diabatic couplings at all the transition-state geometries for the S_1 PES are presented in Table VI. The diabatic couplings along linear-synchronous-transit/bond stretch pathways starting at min1 and min3 present qualitatively the same behavior to those starting at min2 and presented in Fig. 6. In particular, the diabatic couplings between the intersecting states are in the order $(23)>(24)>(34)$ in all three cases. The couplings at the 1-2 TS7, 2-3 TS8 and 3-1 TS9 interconversion transition states are roughly similar to those at the bond rupture transition states. Finally, *trans*-C_s TS10 and *cis*-C_s TS11 present somewhat different and generally smaller diabatic couplings.

IV. DISCUSSION

IV.A. Adiabatic S_0 and S_1 PESs: Comparison with previous studies

The stationary points and energies obtained here for the adiabatic S_0 and S_1 PESs can be compared to those reported in previous theoretical studies. For the ground-state S_0 PES, the structure of the *trans*-C_s conformer has been determined previously.[46,52] Ding *et al.*[52] reported $R_{C-Cl}=1.821$ Å at the CASSCF(8,7)/6−31G* level, in good agreement with our results (1.824 Å, see Table II), while Bacchus-Montabonel *et al.*[46] used CASSCF with an active space of 30 electrons in 18 orbitals to obtain a value (1.786 Å) very close to the experiment [1.789 Å (Ref. 102)]. The partially optimized *gauche* conformer was reported in Ref. 46 with a Br−C_α−C−Cl torsional angle of 61° and a *trans-gauche* barrier of 0.07 eV, comparable to our results of 74° and 0.08 eV (Table II). Dissociation energies from the *trans*-C_s conformer to products are reported by Ding *et al.*[52] at the CASSCF level as 4.2 eV [$Br(^2P)+C_\alpha H_2C(O)Cl(\tilde{A}\,^2A')$] and 2.5 eV [$Cl(^2P)+BrC_\alpha H_2CO(\tilde{X}\,^2A')$]. The products of C_α−Br dissociation with the lowest energy are $Br(^2P)+C_\alpha H_2C(O)Cl(\tilde{X}\,^2A'')$, whereas Ding *et al.* mistakenly assumed that $Br(^2P)+C_\alpha H_2C(O)Cl(\tilde{A}\,^2A')$ is the lowest-energy dissociation channel. With this caveat, the value reported by Ding *et al.* agrees well with that reported here for $Br(^2P)+C_\alpha H_2C(O)Cl(\tilde{A}\,^2A')$ (Table IV). For C–Cl dissociation, there is a discrepancy of about 1 eV between the dissociation energy obtained here, or the experimental energy, and that obtained by Ding *et al.* In this case the electronic states of products assumed by those authors are the same as here. The origin of the discrepancy could be that the active space used by Ding *et al.* (eight electrons in seven orbitals) has limitations for the provision of relative energies, especially since the authors used different active orbitals in different regions of the PESs.

For the excited-state S_1 PES, only a few of the stationary points characterized here have been reported. Thus, *trans*-C_s TS10 was reported by Bacchus-Montabonel *et al.*,[46] and the stationary points here denoted min1, C–Cl TS3, and C–Br TS6 were reported by Ding *et al.*[52] The previously reported geometry of *trans*-C_s TS10 agrees well with that reported in Table IV, with the largest difference being 0.01 Å for the C–Cl distance. The structures of the other stationary points also agree generally well with those reported in Ref. 52, with differences of 0.02–0.04 Å for the C–O and C_α–Br distances, which can again be probably attributed to the different active spaces employed in that study and here.

Table VII presents the S_0-S_1 vertical and adiabatic excitation energies and reaction barriers on the adiabatic S_1 PES computed here and in previous research. Also, the EOM-CCSD method is used to compare the S_0-S_1 excitation energies with those obtained at the 6S-MC-QDPT level. As one can see, in all cases EOM-CCSD excitation energies are systematically higher than the 6S-MC-QDPT ones by 0.1–0.3 eV. The vertical excitation energies from the stable conformers on the S_0 PES are presented for the first two electronic bands to allow for comparison with experiment. If

TABLE VII. Excitation energies in eV computed at the SS-CASSCF geometries. The two first experimental bands are located approximately at 4.6 and 5.9 eV (reported in Fig. 1 of Ref. 32).

	6S-MC-QDPT	EOM-CCSD	CASSCF (Ref. 47)	MRCI (Ref. 52)
trans-C_s (vertical)	5.37(a''), 6.07(a'')	5.41(a''), 6.33(a'')	···	5.41
trans-C_s-*trans*-C_s TS10	4.29(a'')	4.44(a'')	4.38	
trans-C_s-min1	3.92(a)	4.21(a)	4.10	3.91
gauche min (vertical)	4.81(a), 5.48(a)	4.97(a), 5.76(a)	···	
min1-C–Br TS6	0.01(a)			0.25
min1-C–Cl TS3	0.29(a)			0.36

the maxima of the experimental bands can be attributed to vertical excitation from the ground state, the results predict that excitation to S_1 takes place from the *gauche* conformer on S_0, while for excitation to S_2, the vertical energy from the *trans*-C_s conformer is closer to the center of the band observed experimentally.[32] Although the approximation that vertical excitations correspond to electronic absorption band maxima is in general somewhat inaccurate,[114,115] the typical error introduced by this approximation [0.1–0.3 eV (Ref. 115)] is small enough that it does not cast doubt on our assignment of the band maxima. For the adiabatic excitation energies from the *trans*-C_s minimum on the S_0 PES to *trans*-C_s TS10 and min1 on the S_1 PES, the EOM-CCSD results agree better with the values reported by Bacchus-Montabonel *et al.*[46] at the CASSCF level, while the 6S-MC-QDPT results are more in line with the MRCI energies of Ding *et al.*[52]

From the results in Table VII it is possible to estimate the true S_0-S_1 vertical excitation energies. In all previous calculations and also in the present calculations, the basis sets employed are of double-zeta plus polarization quality, which is not expected to yield quantitative energies. The typical accuracy of the MC-QDPT method or the related single-state multireference Møller-Plesset (MRMP) method[61] regarding vertical excitation energies is about 0.25 eV,[116–121] with some tendency to overestimate the excitation energies when small basis sets are employed. On the other hand, the EOM-CCSD method with a medium-sized basis set overestimates the experimental excitation energies by 0.2–0.3 eV on the average.[122–125] The inclusion of triple excitations to EOM-CCSD and extension of the basis set size systematically lower the excitation energies in most cases, reducing the average deviation from experiment to close to 0.1 eV.[122–125] Thus, it is reasonable to expect that the true vertical excitation energies are lower than the EOM-CCSD values by about 0.2–0.3 eV. The corrected first two vertical excitation energies would then be located at 5.1–5.2 and 6.0–6.1 eV for *trans*-C_s min and 4.7–4.8 and 5.5–5.6 eV for *gauche* min (see Table VII). Hence, the MC-QDPT method is likely to afford a good approximation to the true excitation energies even if they are somewhat overestimated by this method.

Bond scission barrier heights were calculated by Ding *et al.*[52] for some of the stationary points found here and are compared with the 6S-MC-QDPT barrier heights in Table VII. Note that the absolute minimum on the S_1 PES is min2 according to our results, but this minimum has not been reported before. The barrier heights for C–Cl dissociation from min1 obtained here and those of Ding *et al.* agree well with each other, but the barrier to C_α–Br fission obtained by us is much lower. Both calculations agree that the C–Cl barrier is significantly higher than the C_α–Br barrier. Previous studies at the MRMP level have found that the effect of the basis set on the barrier heights is modest (sometimes as small as 10% of the barrier height), but the size and composition of the active space are much more important.[62,126,127] In this respect, care was taken in the present study to define a qualitatively correct active space that conserves the character of the active orbitals in all regions of configuration space. We believe that the approach of Ding *et al.*[52] of defining an active space whose orbital composition varies with respect to geometry is prone to give unbalanced results, despite the later inclusion of dynamical correlation at the MRCI level. Of course, it would be desirable to carry out a more systematic study with other high-level *ab initio* methods, especially with larger basis sets, but that is beyond the scope of the present study.

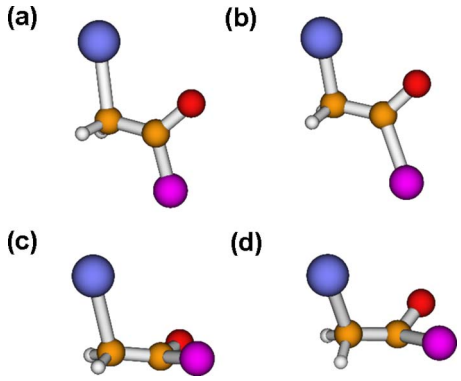

FIG. 7. Illustrations of geometries at avoided crossings. (a) Avoided crossing along C_α–Br dissociation path in Figs. 5(a)–5(c). The C_α–Br distance is 2.4 Å. (b) Avoided crossing along C–Cl dissociation path in Figs. 5(a)–5(d). The C–Cl distance is 2.3 Å. (c) Avoided crossing along C_α–Br dissociation path in Figs. 6(a)–6(c). The C_α–Br distance is 2.4 Å. (d) Avoided crossing along C–Cl dissociation path in Figs. 6(a)–6(d). The C–Cl distance is 2.3 Å.

IV.B. Geometries at avoided crossings

To facilitate the discussion in Sec. IV.C, Fig. 7 illustrates the geometries at the avoided crossings discussed so far. Thus, panels (a) and (b) depict the avoided crossings for the curves shown in Fig. 5, derived from *trans*-C_s TS10 but with a Br–C_α–C–Cl dihedral angle of 170°. Note that in this case there is essentially only one diabatic coupling significantly different from zero for each dissociation coordinate [see Figs. 5(c) and 5(d)], in keeping with the fact that the other two couplings are zero when the molecule contains a plane of symmetry. Note also that the structures in Figs. 7(a) and 7(b) are close neither to the Franck-Condon region nor to the minimum energy path, where the Br–C_α–C–Cl and C_α–C–O–Cl dihedral angles are quite different from those in Figs. 7(a) and 7(b), as discussed in Sec. IV.C. The structures in panels (c) and (d) of Fig. 7 are part of linear-synchronous-transit pathways going through the actual lowest-energy transition states (C–Br TS6 and C–Cl TS4, respectively). Hence, they are expected to be more relevant to the actual reaction mechanism. Note that the $-BrC_\alpha H_2$ group has rotated by about 90° with respect to the structures in panels (a) and (b) (see Table IV), and that two or the three diabatic couplings are significantly different from zero for each dissociation coordinate [see Figs. 6(c) and 6(d)]. These factors could affect the dynamics significantly.

IV.C. Reaction mechanism: Nonadiabaticity of C–Br scission

Figure 8 depicts the Franck-Condon region, the lowest-energy reaction path, and the energies of the ground and first excited states of products for the photodissociation of

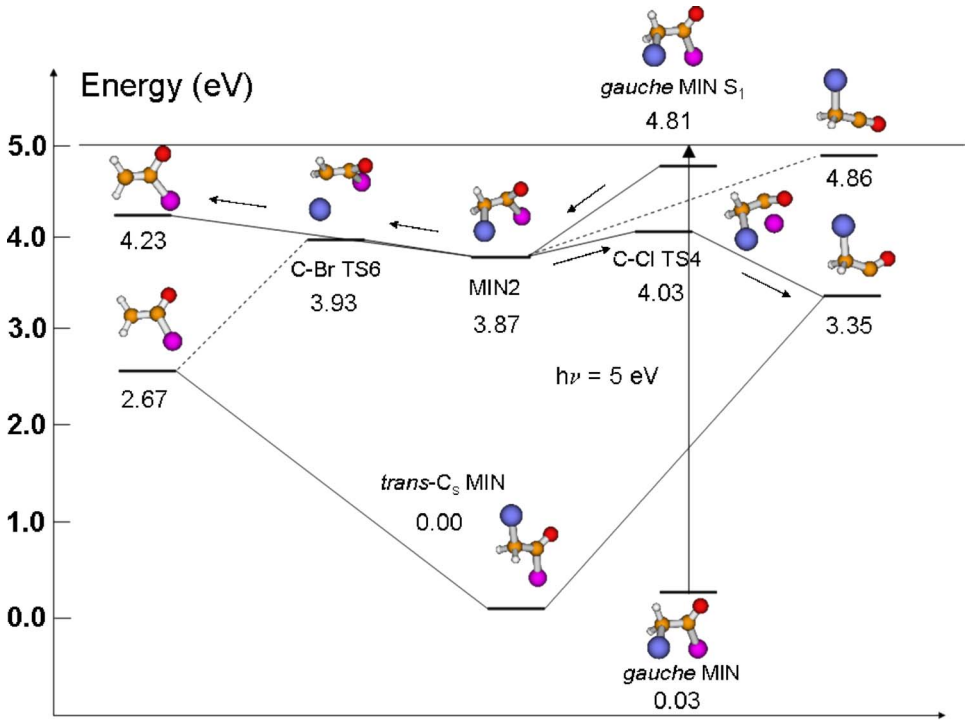

FIG. 8. Schematic representation of the excitation from S_0 to the Franck-Condon region and of the MEP on the S_1 PES. Structures are optimized at the SS-CASSCF level and adiabatic energies computed at the 6S-MC-QDPT level. The adiabatic energies are given in eV relative to the S_0 energy of *trans*-C_s.

$BrC_\alpha H_2C(O)Cl$. To simplify the diagram, only the stationary points required for the following discussion have been depicted. The reaction pathway on the S_1 PES would start close to the Franck-Condon point on the S_1 PES, corresponding to the geometry of *gauche* min on the S_0 PES from which the system is promoted to the S_1 PES. In order to study how feasible it is for the system to evolve directly from the Franck-Condon region towards products without distortion of the molecular backbone, 6S-MC-QDPT calculations of C_α–Br and C–Cl dissociation curves (not presented here) with the rest of the geometric parameters of *gauche* min at their equilibrium values (shown in Table I) were carried out. These calculations predict that the C_α–Br dissociation is feasible from the Franck-Condon geometry, whereas the potential energy maximum along the C–Cl coordinate is above the energetic limit imposed by the energy of the photon (5 eV). Even though the C_α–Br dissociation can proceed without distortion of the rest of the molecule, the energy available for dissociation is rather low [0.19 eV without taking into account the difference in zero-point energy (ZPE) between the ground and the excited state; see Fig. 8 and Table VII]. Instead, a more likely pathway involves geometric relaxation from the Franck-Condon point in order to minimize the potential energy. In order to study the reaction mechanism qualitatively, a steepest-descent path was constructed on the S_1 PES at the SS-CASSCF level starting at the geometry of the *gauche* S_0 conformer. The results show that the C–O bond relaxes to attain its equilibrium bond length on the S_1 PES, accompanied by some stretching of the C_α–Br bond. After relaxation of these bonds, the C_α–C–O–Cl dihedral angle starts to decrease from its ground-state value of close to 180°, due to pyramidalization of the carbonyl C atom, until the system reaches the absolute minimum on the S_1 PES (min2). Both the C–Cl and C_α–Br bond scissions can then take place crossing much lower energy barriers, with the system having gained almost 1 eV of nuclear kinetic energy (see Fig. 8). Other possible reaction pathways would continue from min2 with conversion to the other isomeric minima on S_1 (min1 and min3) and subsequent dissociation, although those pathways are less favorable on energetic grounds (see Figs. 2 and 3).

In photochemical reactions with an adiabatic exit channel barrier, one expects that this barrier, the energy distribution at the barrier, and the exit-valley coupling control the deposition of translational energy into products.[128–131] In particular, one usually expects that most of the potential energy released along the reaction coordinate after passing the barrier is converted to relative translational energy of the photofragments, and that the translational energy distribution is rather insensitive to the total available energy.[108,132–135] In contrast, reactions without an exit channel barrier typically have an asymmetric bell-shaped translational energy distribution with its maximum somewhat away from zero translational energy.[128,130] It can be seen from Fig. 8 that the exit channel barrier formed by C–Cl TS4 (i.e., the barrier with respect to products) is approximately 0.68 eV high at the 6S-MC-QDPT level, in general agreement with the maximum in the relative translational energy distribution $[P(E_T)]$ of products for C–Cl dissociation of bromoacetyl chloride (0.61 eV) found in the experiments of Person *et al.*[32] Also, from the 6S-MC-QDPT energies in Fig. 8 the available energy after photoexcitation at 5 eV would be about 1.65 eV, in qualitative agreement with the experimental $P(E_T)$ extending to slightly beyond 1.3 eV.[32] This is consistent with C–Cl dissociation taking place predominantly along the adiabatic

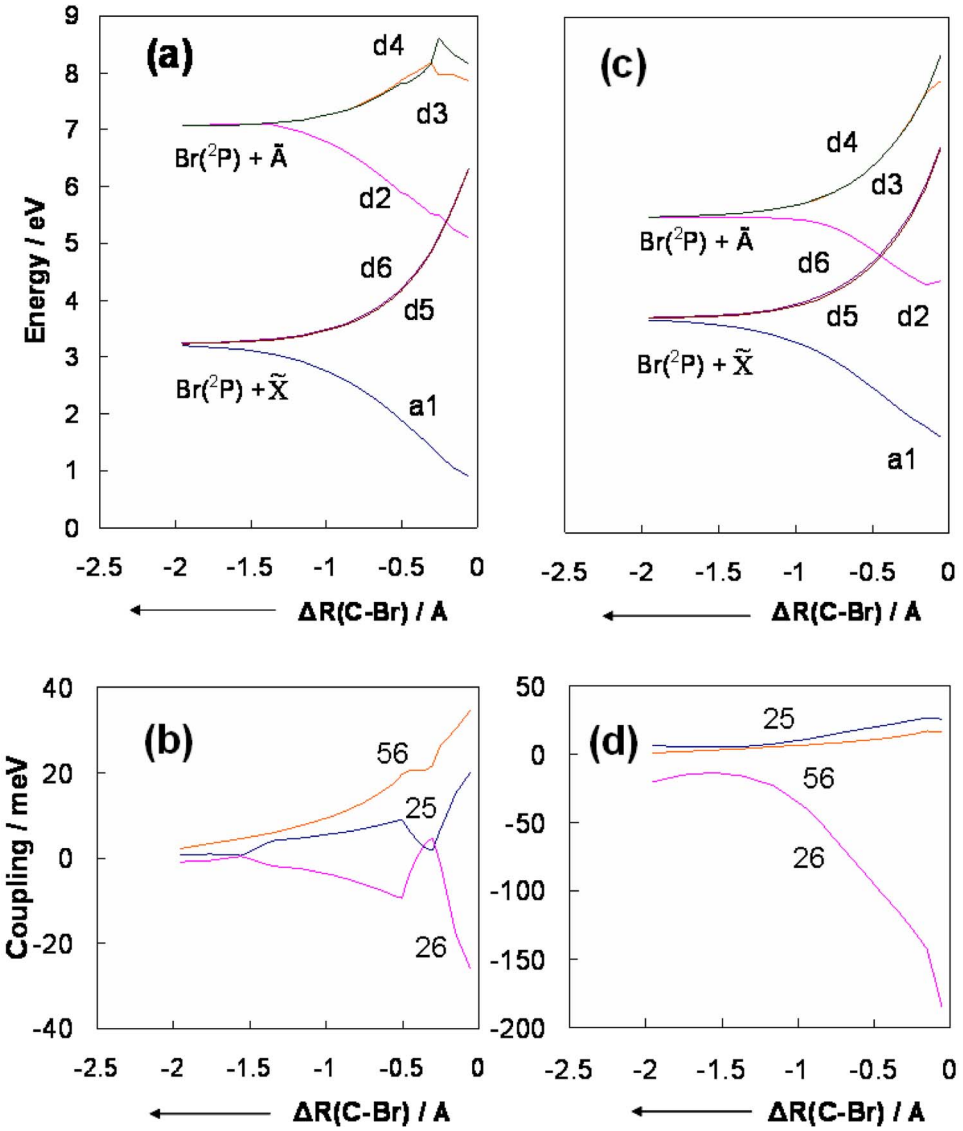

FIG. 9. Potential energy curves and diabatic couplings along the C_α–Br dissociation coordinate at the SA(6)-CASSCF level, starting with all internal coordinates except R(C–O) and Br–C_α–C–Cl at the equilibrium structure of min2 (see Table IV). The C_α–Br bond distances are referred to the respective equilibrium distances of min2, i.e., $\Delta R(C_\alpha\text{–Br}) \equiv 2.046$ Å $- R(C_\alpha\text{–Br})$. The values of the other coordinates are as shown for structure min2 in Table IV. For R(C–O) = 1.188 Å, Br–C_α–C–Cl = 165°: (a) adiabatic ground state and excited diabatic states and (b) diabatic couplings along the C_α–Br coordinate. For R(C–O) = 1.340 Å, Br–C_α–C–Cl = 135°: (c) adiabatic ground state and excited diabatic states and (d) diabatic couplings along the C_α–Br coordinate.

pathway correlating with products in their ground electronic states. A very different conclusion can be drawn for the C_α–Br dissociation. In this case, the relative translational energy distribution was assumed by Kash *et al.* to be the same as that observed in experiments on bromoacetone photodissociation at 308 nm,[35] peaking at about 0.2 eV and extending up to 0.9 eV.[36] However, the exit channel barrier formed by C–Br TS6 (i.e., the energy difference between the top of the barrier and ground-state products computed at the 6S-MC-QDPT level) is about 1.26 eV, as shown in Fig. 8. If the system crosses the barrier adiabatically to produce ground-state radicals, that would mean that less than 20% of the exit channel barrier energy is channeled to relative translation of products, which would be unusual. However, if the dissociation produces excited-state radicals, then a final translational energy peaking at about 0.2 eV corresponds to about 25% of the available energy and a cutoff at 0.9 eV is close to the expected cutoff of about 0.8 eV.

The evidence presented in the last paragraph strongly suggests that most of the reactive flux in the C_α–Br dissociation process goes through the diabatic pathway that correlates with the excited states of products. That would imply that nonadiabatic effects are very large for the C_α–Br scission, but that the reaction proceeds along the energetically allowed diabatic pathway to excited-state products instead of being nonadiabatically suppressed as assumed in previous studies. For $BrC_\alpha H_2C(O)Cl$ this possibility does not seem to have been taken into account previously. Along the MEP, the magnitude of the SA-CASSCF diabatic couplings at the electronic state intersections in the C–Cl coordinate are more than a factor of 10 larger than for the C_α–Br coordinate (see above). The magnitudes of the diabatic couplings at other relevant geometries are illustrated in Fig. 9 for the C_α–Br coordinate and in Fig. 10 for the C–Cl coordinate. The dissociation curves originate from two geometries derived from the absolute minimum on the S_1 PES (min2), the first one with a C–O distance of 1.188 Å and a Br–C_α–C–Cl dihedral angle of 165° and the second one with a C–O distance of 1.340 Å and a Br–C_α–C–Cl dihedral angle of 135°. Figure 9 shows the diabatic energies and couplings along the C_α–Br coordinate. The diabatic couplings for the first geometry are comparable in magnitude to those along the MEP (see Fig. 6), as are two of the couplings for the second geometry, with one of them (i.e., U_{26}) being significantly larger. The diabatic

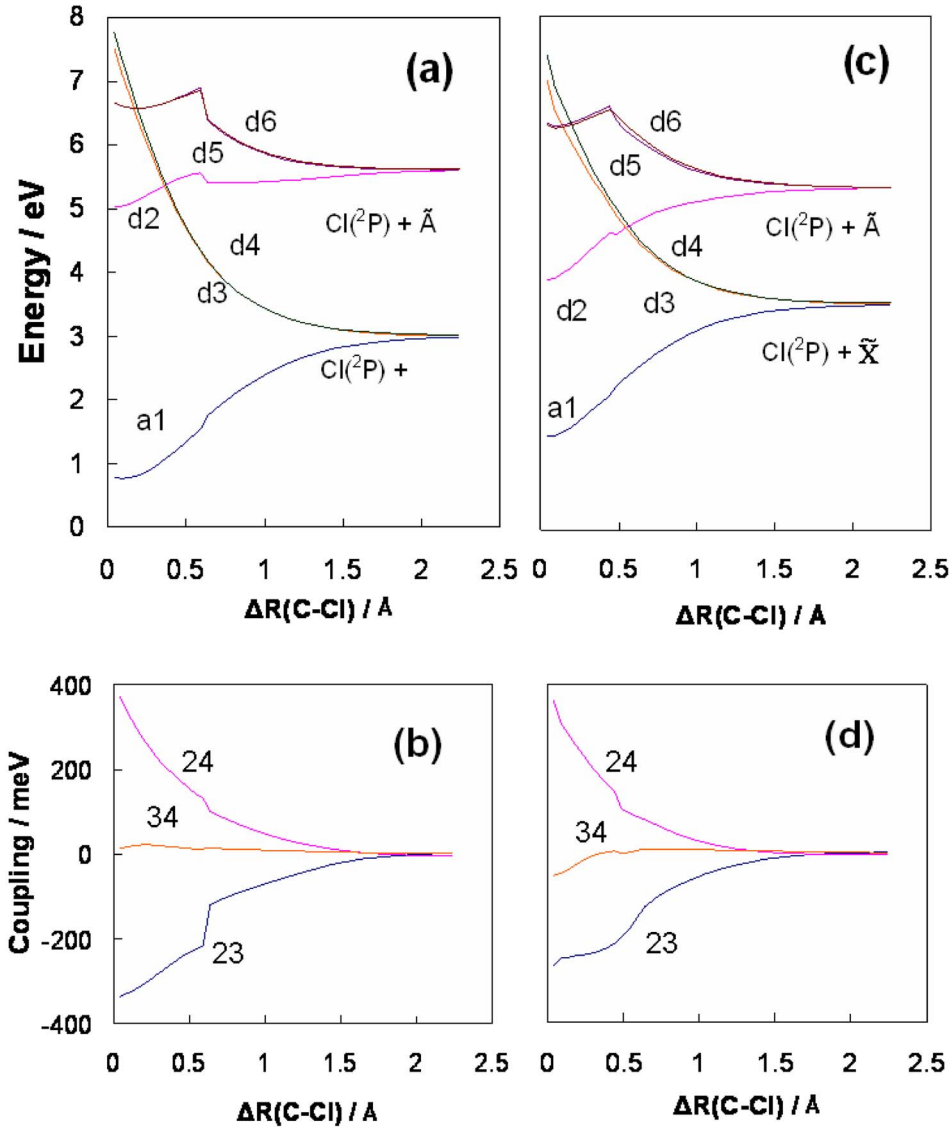

FIG. 10. Potential energy curves and diabatic couplings along the C_α–Br dissociation coordinate at the SA(6)-CASSCF level, starting with all internal coordinates except R(C–O) and Br–C_α–C–Cl at the equilibrium structure of min2 (see Table IV). The C–Cl bond distances are referenced to the respective equilibrium distances of min2, i.e., ΔR(C–Cl) $\equiv R$(C–Cl) – 1.760 Å. The values of the other coordinates are as shown for structure min2 in Table IV. For R(C–O) = 1.188 Å, Br–C_α–C–Cl = 165°: (a) adiabatic ground state and excited diabatic states, and (b) diabatic couplings along the C–Cl coordinate. For R(C–O) = 1.340 Å, Br–C_α–C–Cl = 135°: (c) adiabatic ground state and excited diabatic states, and (d) diabatic couplings along the C–Cl coordinate.

couplings along the C–Cl coordinate are presented in Fig. 10. For the two combinations of C–O distance and Br–C_α–C–Cl dihedral angle in the figure, the magnitudes of the couplings are comparable to those along the MEP shown in Fig. 6. The geometries at the avoided crossings in Figs. 9(a) and 10(a) are similar to those in Fig. 7(a) and 7(b) except that in Fig. 9 the C–O distance is typical of ground-state geometries and the C_α–C–O–Cl dihedral angle is typical of excited-state geometries. The geometries at the avoided crossings in Figs. 9(c) and 10(c) resemble more those in Figs. 7(c) and 7(d), as the former geometries are near the minimum energy path on the S_1 PES. This is also consistent with the avoided crossings in Figs. 9(c) and 10(c) being energetically more accessible than those in Figs. 9(a) and 10(a).

From the dissociation curves constructed above, one can conclude that the magnitude of the diabatic coupling for the C_α–Br coordinate is such that, according to an estimate of Waschewsky *et al.*[36] based on a one-dimensional Landau-Zener model, less than 5% of the trajectories should cross the barrier adiabatically. Although one-dimensional models are not reliable for multidimensional systems,[45] the magnitude of the diabatic couplings does support the conclusion that C–Cl dissociation proceeds adiabatically and C_α–Br dissociation proceeds diabatically.

In order to further assess the validity of this conclusion, other factors should be taken into account. For instance, it could be argued that if there is a large geometrical distortion between the transition state and products, a large fraction of the energy could be channeled to vibration and rotation of the molecular products rather than into relative translation. In this case, the $P(E_T)$ distribution could peak at low translational energies even if the system follows an adiabatic pathway to dissociation. Considerable vibrational excitation in $C_\alpha H_2C(O)Cl$ would indeed be expected if the C_α–Br photodissociation proceeds adiabatically, due to significant changes in the C–C and C–O bond distances from C–Br TS6 to ground-state $C_\alpha H_2C(O)Cl$ (Tables II and IV). The rotational energy imparted to the $C_\alpha H_2C(O)Cl$ fragment could also be potentially large, since the large mass of the cofragment (the Br atom) and angular momentum conservation mean that the rotational angular momentum can vary in a relatively wide range. An example of large rotational energy

release in this context is provided by photodissociation of CH_3OCl.[136] In general, for negligible angular momentum in the parent, the rotational angular momentum of the recoiling fragments should be approximately equal to their orbital angular momentum. In analyzing the photodissociation of CH_3OCl, an impulsive kinetic energy release was assumed between the Cl and the O atom in the CH_3O portion of the molecule; this predicted a rotational energy of about 0.8 eV for CH_3O. We applied this model to $BrC_\alpha H_2C(O)Cl$ at the geometry of C–Br TS6, and we obtained a rotational energy of only 0.09 eV for the $C_\alpha H_2C(O)Cl$ fragment, much lower than for CH_3O. This result is due to the lower translational energy release [the maximum in the distribution is at about 0.2 eV for $BrC_\alpha H_2C(O)Cl$ (Ref. 36) vs 2.1 eV for CH_3OCl (Ref. 136)], the larger reduced mass of the $Br–C_\alpha H_2C(O)Cl$ system, and the larger moment of inertia of the $C_\alpha H_2C(O)Cl$ fragment. We conclude that rotational energy release should not affect the product energy distribution of C–Br dissociation significantly.

Regarding the vibrational energy release, there are examples in the literature of reactions with exit channel barriers and strong geometrical distortion between the transition state and products, where at least 60% of the potential energy from the top of the barrier is converted into relative product translation.[133,135] Since about 60% of the 1.25 eV exit channel barrier would go into product relative translation if the C_α–Br photodissociation proceeded adiabatically, the peak in the $P(E_T)$ distribution should be at 0.75 eV or higher, instead of 0.2 eV as observed experimentally. Another comparison can be made to a system that presents similar characteristics to $BrC_\alpha H_2C(O)Cl$, e.g., photodissociation of methyl vinyl ether at 193 nm to yield vinoxy (CH_2CHO) and methyl (CH_3) radicals.[137] Two peaks were observed in the experimental $P(E_T)$, one less intense peak with large translational energy and a maximum at more than 2 eV, assigned to $CH_3(\tilde{X})+CH_2CHO(\tilde{X}\,^2A'')$, and another much more intense peak with low E_T peaking at about 0.3 eV, assigned to $CH_3(\tilde{X})+CH_2CHO(\tilde{A}\,^2A')$. The similarity of these assignments with the adiabatic $[Br(^2P)+C_\alpha H_2C(O)Cl(\tilde{X}\,^2A'')]$ and diabatic $[Br(^2P)+C_\alpha H_2C(O)Cl(\tilde{A}\,^2A')]$ C_α–Br dissociation channels in bromoacetyl chloride is compelling, as is the qualitative agreement between the $P(E_T)$ for the excited-state channels, peaking at 0.2 eV for bromoacetyl chloride and at 0.3 eV for methyl vinyl ether.

Assuming that C_α–Br dissociation in $BrC_\alpha H_2C(O)Cl$ proceeds diabatically gives us a hint as to why the experimental Cl:Br branching ratio is 1.0:0.4, favoring Cl production. As seen in Fig. 8, the energy required to surmount the C–Cl TS4 barrier adiabatically (4.03 eV) is *lower* than the energy required (4.23 eV) for diabatic C_α–Br bond scission. Note that diabatic C_α–Br bond scission proceeds without a barrier (see Figs. 5 and 6); therefore the required energy is just the energy of excited-state products. It is interesting to note that the experimental Cl:Br branching ratio for bromopropionyl chloride [1.0: <0.05 (Ref. 33)] is significantly larger than for bromoacetyl chloride. This observation is consistent with the even smaller magnitude[33,36] of the theoretical diabatic coupling at the C_α–Br avoided crossing for bromopropionyl chloride (5–10 cm^{-1}, i.e., 0.6–1.2 meV) and with the much larger magnitude[33,36] of the coupling along the C–Cl coordinate (50–250 cm^{-1}, i.e., 6–31 meV). Whether or not the experimental results can be interpreted in a similar way as for bromoacetyl chloride depends on the dissociation energies for diabatic C_α–Br fission and adiabatic C–Cl fission. This point deserves further scrutiny but is beyond the scope of the present study.

Assuming that the C_α–Br dissociation takes place diabatically and the C–Cl dissociation adiabatically and considering the energy requirements for dissociation, a RRKM calculation would predict that C–Cl dissociation is preferred over C_α–Br dissociation in $BrC_\alpha H_2C(O)Cl$. However, the actual dynamics might well involve other complications, such as incomplete intramolecular energy redistribution, as suggested by Ding *et al.*[52] Nevertheless, the fact that the energy requirement for diabatic C_α–Br dissociation is larger than that for adiabatic C–Cl dissociation should be decisive in explaining why the C–Cl dissociation is favored in the experiments despite its larger adiabatic barrier, and the present diabatic surfaces and couplings are a first step toward carrying out multidimensional dynamics calculations to explore this competition.

V. CONCLUSIONS

The adiabatic and diabatic singlet electronic states relevant to C_α–Br and C–Cl photodissociation of $BrC_\alpha H_2C(O)Cl$ have been studied with a combination of CASSCF and MC-QDPT methods. The dissociation energies and the S_0-S_1 excitation energies computed at the 6S-MC-QDPT level are rather accurate, with maximum discrepancies of about 10% of the absolute values. The deviations are mainly due to the modest size of the basis set employed. This accuracy is sufficient to draw conclusions regarding the reaction mechanism.

The minimum energy path predicted at the SS-CASSCF level on the S_1 PES after excitation at the geometry of the *gauche* S_0 conformer mainly involves relaxation of the carbonyl bond and the C_α–C–O–Cl dihedral angle to reach the pyramidal (with respect to the carbonyl C atom) absolute minimum on the S_1 PES. The system can then surmount the relatively low adiabatic barriers along the C–Cl and C_α–Br bond dissociation coordinates. Three electronic states (S_1, S_2, and S_3) form energetically allowed intersections along each of the C–Cl and C_α–Br coordinates for the nonsymmetrical geometries relevant to the dynamics.

The main new conclusions of this study are derived from a comparison between the kinetic energy release expected on the basis of the present 6S-MC-QDPT adiabatic potential energies and SA-CASSCF diabatic couplings and the kinetic energy release observed in the experiments. This comparison revealed that the C–Cl dissociation probably proceeds adiabatically to ground-state products, but the C_α–Br dissociation probably follows a diabatic pathway to the energetically accessible excited-state products. Therefore, nonadiabatic effects probably dominate the C_α–Br scission, but the reaction proceeds along a diabatic pathway to products instead of being nonadiabatically suppressed as proposed in previous

theoretical studies. This interpretation is consistent with the SA-CASSCF diabatic couplings along the MEP being more than a factor of 10 larger for C–Cl bond breaking than for C_α–Br bond breaking. For the latter, the magnitude of the diabatic couplings is consistent with an almost complete suppression of adiabatic C_α–Br scission, lending support to the above conclusion. Based on these findings, a new factor that is likely to strongly influence the experimental branching ratio (Cl:Br=1.0:0.4) has been uncovered: the adiabatic C–Cl dissociation is energetically more favorable than the diabatic C_α–Br dissociation. Work is beginning on semiclassical dynamics on multidimensional potential energy surfaces in order to assess these conclusions. This work will be facilitated by the fact that the diabatic surfaces and couplings calculated here are smooth functions of geometry and can be represented by multidimensional analytic functions based on interpolation.

ACKNOWLEDGMENTS

The authors are grateful to Mark S. Gordon for permission to port the ISA algorithm from GAMESS to HONDOPLUS. This work was supported in part by the National Science Foundation under Grant No. CHE03-49122.

[1] A. W. Jasper, C. Zhu, S. Nangia, and D. G. Truhlar, Faraday Discuss. **127**, 1 (2004).
[2] E. Teller, J. Phys. Chem. **41**, 109 (1937).
[3] F. Bernardi, M. Olivucci, and M. A. Robb, Chem. Soc. Rev. **25**, 321 (1996).
[4] D. R. Yarkony, J. Phys. Chem. A **105**, 6277 (2001).
[5] D. G. Truhlar and C. A. Mead, Phys. Rev. A **68**, 032501 (2003).
[6] G. A. Worth and L. S. Cederbaum, Annu. Rev. Phys. Chem. **55**, 127 (2004).
[7] C. A. Mead and D. G. Truhlar, J. Chem. Phys. **77**, 6090 (1982).
[8] B. K. Kendrick, C. A. Mead, and D. G. Truhlar, Chem. Phys. **277**, 31 (2002).
[9] F. T. Smith, Phys. Rev. **179**, 111 (1969).
[10] T. F. O'Malley, Adv. At. Mol. Phys. **7**, 223 (1971).
[11] A. Macias and A. Riera, J. Phys. B **11**, 2489 (1978).
[12] B. C. Garret and D. G. Truhlar, in *Theoretical Chemistry: Advances and Perspectives*, edited by D. Henderson (Academic, New York, 1981), Vol 6 A, p. 215 [Theor. Chem. (N.Y.) 6A ("Theory of Scattering: Papers in Honor of Henry Eyring"), p. 215 (1981)].
[13] J. B. Delos, Rev. Mod. Phys. **53**, 287 (1981).
[14] H.-J. Werner and W. Meyer, J. Chem. Phys. **74**, 5802 (1981).
[15] M. Baer, in *Theory of Chemical Reaction Dynamics*, edited by M. Baer (CRC, Boca Raton, FL, 1985), Vol. 2, p. 219.
[16] R. Cimiraglia, J.-P. Malrieu, M. Persico, and F. Spiegelmann, J. Phys. B **18**, 3073 (1985).
[17] T. Pacher, L. S. Cederbaum, and H. Köppel, J. Chem. Phys. **89**, 7367 (1988).
[18] V. Sidis, in *Collision Theory for Atoms and Molecules*, edited by F. A. Gianturco (Plenum, New York, 1989), p. 343.
[19] W. Domcke and C. Woywood, Chem. Phys. Lett. **216**, 362 (1993).
[20] R. J. Cave and M. D. Newton, J. Chem. Phys. **106**, 9213 (1997).
[21] R. Thürwächter and P. Halvick, Chem. Phys. **221**, 33 (1997).
[22] G. J. Atchity and K. Ruedenberg, Theor. Chem. Acc. **97**, 47 (1997).
[23] M. Yang and M. H. Alexander, J. Chem. Phys. **107**, 7148 (1997).
[24] V. M. García, M. Reguero, R. Caballol, and J.-P. Malrieu, Chem. Phys. Lett. **281**, 161 (1997).
[25] T. Klüner, S. Thiel, and V. Staemmler, J. Phys. B **32**, 4931 (1999).
[26] H. Nakamura and D. G. Truhlar, J. Chem. Phys. **115**, 10353 (2001).
[27] M. P. Fülscher and L. Serrano-Andrés, Mol. Phys. **100**, 903 (2002).
[28] A. Troisi and G. Orlandi, J. Chem. Phys. **118**, 5356 (2003).
[29] A. W. Jasper, B. K. Kendrick, C. A. Mead, and D. G. Truhlar, Adv. Ser. Phys. Chem. **14**, 329 (2004).
[30] H. Köppel, Adv. Ser. Phys. Chem. **15**, 175 (2004).
[31] M. D. Person, P. W. Kash, S. A. Schofield, and L. J. Butler, J. Chem. Phys. **95**, 3843 (1991).
[32] M. D. Person, P. W. Kash, and L. J. Butler, J. Chem. Phys. **97**, 355 (1992).
[33] P. W. Kash, G. C. G. Waschewsky, L. J. Butler, and M. M. Francl, J. Chem. Phys. **99**, 4479 (1993).
[34] P. W. Kash, G. C. G. Waschewsky, and L. J. Butler, J. Chem. Phys. **100**, 4017 (1994).
[35] P. W. Kash, G. C. G. Waschewsky, R. E. Morss, L. J. Butler, and M. M. Francl, J. Chem. Phys. **100**, 3463 (1994).
[36] G. C. G. Waschewsky, P. W. Kash, T. L. Myers, D. C. Kitchen, and L. J. Butler, J. Chem. Soc., Faraday Trans. **90**, 1581 (1994).
[37] P. W. Browning, D. C. Kitchen, M. F. Arendt, and L. J. Butler, J. Phys. Chem. **100**, 7765 (1996).
[38] T. L. Myers, D. C. Kitchen, B. Hu, and L. J. Butler, J. Chem. Phys. **104**, 5446 (1996); J. Chem. Phys. **105**, 2948(E) (1996).
[39] N. R. Forde, T. L. Myers, and L. J. Butler, Faraday Discuss. **108**, 221 (1997).
[40] L. J. Butler, Annu. Rev. Phys. Chem. **49**, 125 (1998).
[41] Y. Liu and L. J. Butler, J. Chem. Phys. **121**, 11016 (2004).
[42] R. B. Woodward and R. Hoffmann, J. Am. Chem. Soc. **87**, 3951 (1965).
[43] E. E. Nikitin, in *Theory of Elementary Atomic and Molecular Processes in Gases* (Oxford University Press, Oxford, 1974).
[44] C. Y. Zhu, H. Kamisaka, and H. Nakamura, Adv. Chem. Phys. **117**, 127 (2001).
[45] S. L. Mielke, G. J. Tawa, D. G. Truhlar, and D. W. Schwenke, Chem. Phys. Lett. **234**, 57 (1995).
[46] M.-C. Bacchus-Montabonel, N. Vaeck, B. Lasorne, and M. Desouter-Lecomte, Chem. Phys. Lett. **374**, 307 (2003).
[47] B. Lasorne, M.-C. Bacchus-Montabonel, N. Vaeck, and M. Desouter-Lecomte, J. Chem. Phys. **120**, 1271 (2004).
[48] A. J. Marks, J. Chem. Phys. **114**, 1700 (2001).
[49] S. S. Xantheas, G. J. Atchity, S. T. Elbert, and K. Ruedenberg, J. Chem. Phys. **94**, 8054 (1991).
[50] B. O. Roos, M. Fulscher, M. Merchán, and L. Serrano-Andrés, in *Quantum Mechanical Electronic Structure Calculations with Chemical Accuracy*, edited by S. R. Langhoff (Kluwer, Dordrecht, 1995), p. 357.
[51] M. W. Schmidt and M. S. Gordon, Annu. Rev. Phys. Chem. **49**, 233 (1998).
[52] W.-J. Ding, W.-H. Fang, R.-Z. Liu, and D.-C. Fang, J. Chem. Phys. **117**, 8745 (2002).
[53] H. Nakamura and D. G. Truhlar, J. Chem. Phys. **117**, 5576 (2002).
[54] H. Nakamura and D. G. Truhlar, J. Chem. Phys. **118**, 6816 (2003).
[55] A. C. Wahl and G. Das, in *Methods of Electronic Structure Theory*, edited by H. F. SchaeferIII (Plenum, New York, 1977).
[56] R. J. Buenker and S. D. Peyerimhoff, in *New Horizons of Quantum Chemistry*, edited by P.-O. Lowdin and P. Pullman (Reidel, New York, 1976), p. 183.
[57] I. Shavitt, in *Methods of Electronic Structure Theory*, edited by H. F. Schaeffer III (Plenum, New York, 1977), p. 189.
[58] H.-J. Werner, Adv. Chem. Phys. **69**, 1 (1987).
[59] C. W. Bauschlicher, S. R. Langhoff, and P. R. Taylor, Adv. Chem. Phys. **77**, 103 (1990).
[60] H. Lischka, R. Shepard, R. M. Pitzer *et al.*, Phys. Chem. Chem. Phys. **3**, 664 (2001).
[61] K. Hirao, Chem. Phys. Lett. **190**, 374 (1992); , *ibid.* **196**, 397 (1992); K. Hirao, Int. J. Quantum Chem., Quantum Chem. Symp. **26**, 517 (1992);
[62] H. Nakano, K. Nakagama, K. Hirao, and M. Dupuis, J. Chem. Phys. **106**, 4912 (1997).
[63] H. Nakano, J. Chem. Phys. **99**, 7983 (1993). H. Nakano, Chem. Phys. Lett. **207**, 372 (1993).
[64] P. M. Kozlowski and E. R. Davidson, J. Chem. Phys. **100**, 3672 (1994).
[65] J. P. Malrieu, J.-L. Heully, and A. Zaitsevskii, Theor. Chim. Acta **90**, 167 (1995).
[66] B. O. Roos, K. Andersson, M. P. Fülscher, P.-Å. Malmqvist, L. Serrano-Andrés, K. Pierloot, and M. Merchán, Adv. Chem. Phys. **93**, 219 (1996).
[67] C. Angeli, R. Cimiraglia, M. Persico, and A. Toniolo, Theor. Chem. Acc. **98**, 57 (1997).
[68] J. Finley, P.-Å. Malmqvist, B. O. Roos, and L. Serrano-Andrés, Chem. Phys. Lett. **288**, 299 (1998).
[69] H. Nakano, T. Nakajima, T. Tsuneda, and K. Hirao, J. Mol. Struct. **573**, 91 (2001).
[70] K. K. Docken and J. Hinze, J. Chem. Phys. **57**, 4928 (1972).

[71] K. Ruedenberg, L. M. Cheung, and S. T. Elbert, Int. J. Quantum Chem. **16**, 1069 (1979).
[72] H.-J. Werner and M. Meyer, J. Chem. Phys. **74**, 5794 (1981).
[73] R. N. Diffenderfer and D. R. Yarkony, J. Phys. Chem. **86**, 5098 (1982).
[74] T. Rozgonyi, T. Feurer, and L. González, Chem. Phys. Lett. **350**, 155 (2001).
[75] J. Huang, D. Xu, J. S. Francisco, and W. M. Jackson, J. Chem. Phys. **119**, 3661 (2003).
[76] NIST chemistry webbook (http://webbook. nist. gov/chemistry).
[77] U. Meier and V. Staemmler, Theor. Chim. Acta **76**, 95 (1989).
[78] P. C. Hariharan and J. A. Pople, Theor. Chim. Acta **28**, 213 (1973); M. M. Francl, W. J. Pietro, W. J. Hehre, J. S. Binkley, M. S. Gordon, D. J. DeFrees, and J. A. Pople, J. Chem. Phys. **77**, 3654 (1982); R. C. Binning, Jr. and L. A. Curtiss, J. Comput. Chem. **11**, 1206 (1990).
[79] H. A. Witek, Y.-K. Choe, J. P. Finley, and K. Hirao, J. Comput. Chem. **10**, 957 (2002).
[80] D. Rowe, Rev. Mod. Phys. **40**, 153 (1968).
[81] H. Sekino and R. J. Bartlett, Int. J. Quantum Chem., Quantum Chem. Symp. **18**, 255 (1984).
[82] J. Geertsen, M. Rittby, and R. J. Bartlett, Chem. Phys. Lett. **164**, 57 (1989).
[83] H. Koch, H. J. A. Jensen, P. Jørgensen, and T. Helgaker, J. Chem. Phys. **93**, 3345 (1990).
[84] J. F. Stanton and R. J. Bartlett, J. Chem. Phys. **98**, 7029 (1993).
[85] P. J. Knowles, C. Hampel, and H. J. Werner, J. Chem. Phys. **99**, 5219 (1993).
[86] J. Cizek, Adv. Chem. Phys. **14**, 35 (1969).
[87] R. J. Bartlett and J. F. Stanton, Rev. Comput. Chem. **5**, 65 (1994).
[88] K. Raghavachari, G. W. Trucks, J. A. Pople, and M. Head-Gordon, Chem. Phys. Lett. **157**, 479 (1989).
[89] T. H. Dunning, Jr., J. Chem. Phys. **90**, 1007 (1989); D. E. Woon and T. H. Dunning, Jr., *ibid.* **98**, 1358 (1993); A. K. Wilson, D. E. Woon, K. A. Peterson, and T. H. Dunning, Jr., *ibid.* **110**, 7667 (1999).
[90] D. G. Truhlar, Chem. Phys. Lett. **294**, 45 (1998).
[91] P. L. Fast, M. L. Sánchez, and D. G. Truhlar, J. Chem. Phys. **111**, 2921 (1999).
[92] H. Nakamura, J. D. Xidos, J. D. Thompson *et al.*, HONDOPLUS-V4.7, based on HONDO-V99.6, University of Minnesota, Minneapolis, MN, 2006.
[93] M. Dupuis, A. Marquez, and E. R. Davidson, HONDO 99.6, based on HONDO 95.3; M. Dupuis, A. Marquez, and E. R. Davidson, Quantum Chemistry Program Exchange (QCPE), Indiana University, Bloomington, IN 47405, 1999.
[94] J. F. Stanton, J. Gauss, D. Watts *et al.*, ACESII, a program product of the Quantum Theory Group, University of Florida. Integral packages included are the following: J. Almlof and P. R. Taylor, VMOL; P. R. Taylor, VPROPS; and T. Helgaker, H. J. Aa. Jensen, P. Jorgensen, J. Olsen, and P. R. Taylor, ABACUS.
[95] H.-J. Werner, P. J. Knowles, R. Lindh *et al.*, MOLPRO, Version 2002.6, a package of *ab initio* programs (see http://www.molpro. net), Birmingham, UK, 2003.
[96] G. J. Atchity and K. Ruedenberg, J. Chem. Phys. **99**, 3790 (1993).
[97] K. Ruedenberg and G. J. Atchity, J. Chem. Phys. **99**, 3799 (1993).
[98] S. Nangia and D. G. Truhlar, J. Chem. Phys. **124**, 124309 (2006).
[99] R. Valero, Z. H. Li, and D. G. Truhlar Theor. Chem. Acc. (to be published).
[100] T. A. Halgren and W. N. Lipscomb, Chem. Phys. Lett. **49**, 225 (1977).
[101] M. W. Schmidt, K. K. Baldridge, J. A. Boatz *et al.*, J. Comput. Chem. **14**, 1347 (1993).
[102] O. Steinnes, Q. Shen, and K. Hagen, J. Mol. Struct. **66**, 181 (1980).
[103] J. R. Durig, H. V. Phan, and T. S. Little, J. Mol. Struct. **197**, 187 (1989).
[104] I. Nagakawa, I. Ichishima, K. Kuratani, T. Miyazwa, T. Shimanouchi, and S.-I. Mishuzima, J. Chem. Phys. **20**, 1720 (1952).
[105] E. S. Huyser, D. Feller, W. T. Borden, and E. R. Davidson, J. Am. Chem. Soc. **104**, 2956 (1981).
[106] M. Dupuis, J. J. Wendoloski, and W. A. Lester, Jr., J. Chem. Phys. **76**, 488 (1982).
[107] L. F. DiMauro, M. Heaven, and T. A. Miller, J. Chem. Phys. **81**, 2339 (1984).
[108] D. L. Osborn, H. Choi, D. H. Mordaunt, R. T. Bise, D. M. Neumark, and C. M. Rohlfing, J. Chem. Phys. **106**, 3049 (1997).
[109] S. Matsika and D. R. Yarkony, J. Chem. Phys. **117**, 7198 (2002).
[110] H. E. Hunziker, H. Kneppe, and H. R. Wendt, J. Photochem. **17**, 377 (1981).
[111] E. W.-G. Diau, C. Kötting, T. I. Sølling, and A. H. Zewail, ChemPhysChem **3**, 57 (2002).
[112] S. J. Blanksby and G. B. Ellison, Acc. Chem. Res. **36**, 255 (2003).
[113] E. Arunan, J. Phys. Chem. A **101**, 4838 (1997).
[114] E. R. Davidson and A. Jarzecki, Chem. Phys. Lett. **155**, 285 (1998).
[115] O. Christiansen, T. A. Ruden, K. Ruud, and T. Helgaker, J. Chem. Phys. **116**, 8334 (2002).
[116] K. Nakayama, H. Nakano, and K. Hirao, Int. J. Quantum Chem. **66**, 157 (1998).
[117] K. Hirao, H. Nakano, and T. Hashimoto, Chem. Phys. Lett. **235**, 430 (1995).
[118] T. Hashimoto, H. Nakano, and K. Hirao, J. Chem. Phys. **104**, 6244 (1996).
[119] T. Hashimoto, H. Nakano, and K. Hirao, J. Mol. Struct. **451**, 25 (1998).
[120] H. Nakano, T. Tsuneda, T. Hashimoto, and K. Hirao, J. Chem. Phys. **104**, 2312 (1996).
[121] Y. Kawashima, T. Hashimoto, H. Nakano, and K. Hirao, Theor. Chem. Acc. **102**, 49 (1999).
[122] J. D. Watts, S. R. Gwaltney, and R. J. Bartlett, J. Chem. Phys. **105**, 6979 (1996).
[123] J. E. Del Bene, J. D. Watts, and R. J. Bartlett, J. Chem. Phys. **106**, 6051 (1997).
[124] S. A. Kucharski, M. Włoch, M. Musiał, and R. J. Bartlett, J. Chem. Phys. **115**, 8263 (2001).
[125] Y. J. Bomble, K. W. Sattelmeyer, J. F. Stanton, and J. Gauss, J. Chem. Phys. **121**, 5236 (2004).
[126] O. Setokuchi, S. Matuzawa, and Y. Shimizu, Chem. Phys. Lett. **284**, 19 (1998).
[127] P. Gamallo, M. González, and R. Sayós, J. Chem. Phys. **118**, 10602 (2003).
[128] J. T. Cheung, J. D. McDonald, and D. R. Hershbach, Faraday Discuss. Chem. Soc. **55**, 377 (1973).
[129] R. A. Marcus, Faraday Discuss. Chem. Soc. **55**, 379 (1973).
[130] L. Bonnet and J. C. Rayez, J. Chem. Phys. **102**, 9512 (1995).
[131] L. Bonnet, P. Larrégaray, and J. C. Rayez, Phys. Chem. Chem. Phys. **7**, 3540 (2005).
[132] S. S. Hunnicutt, L. D. Waits, and J. A. Guest, J. Phys. Chem. **95**, 563 (1991).
[133] S. W. North, D. A. Blank, J. D. Gezelter, C. A. Longfellow, and Y. T. Lee, J. Chem. Phys. **102**, 4447 (1995).
[134] R. J. Horwitz, J. S. Francisco, and J. A. Guest, J. Phys. Chem. A **101**, 1231 (1997).
[135] D. H. Mordaunt, D. L. Osborn, and D. M. Neumark, J. Chem. Phys. **108**, 2448 (1998).
[136] M. J. Krisch, L. R. McCunn, K. Takematsu, L. J. Butler, F. R. Blase, and J. Shu, J. Phys. Chem. A **108**, 1650 (2004).
[137] M. L. Morton, D. E. Szpunar, and L. J. Butler, J. Chem. Phys. **115**, 204 (2001).